University of Zurich[UZH]

Model-Based Quality Assessment of Tower-Based Field Spectroscopy Measurements

GEO 610 Master's Thesis

Author
Jonas Michel
17-715-723

Supervised by
Prof. Dr. Alexander Damm
Bastian Buman (bastian.buman@gmx.ch)

Faculty representative
Prof. Dr. Alexander Damm

26.07.2022
Department of Geography, University of Zurich

Abstract

Recent and upcoming satellite missions providing high-quality spectrometric measurements are used for vegetation monitoring and studies of ecosystem functioning which are becoming increasingly important in the context of climate change. The calibration and validation of these measurements are crucial but remain a challenge. The need for in-situ references is high and is expected to increase with the trend toward mini-satellites without onboard calibration systems. In-situ measurements however need to be validated themselves before being used as a reference for air- or space-borne sensors. Cross-validation of measurements with additional independent measurements is established but costly. Three approaches using two Radiative Transfer Models (RTM) namely the library for Radiative transfer (libRadtran) and the Soil Canopy Observation of Photosynthesis and Energy Fluxes Model (SCOPE) were built to validate in-situ irradiance and radiance measurements based on simulations. The performance of the approaches was assessed from summer to late autumn and over a single clear-sky day resulting in an average Root Mean Square Relative Error (RMSRE) of below 10% for irradiance simulations and 10%-38% RMSRE for radiance simulations compared to in-situ measurements. The higher RMSRE of radiance simulations originates in misspecifications of the reflectance spectrum which is either assumed constant (approach 1) or modelled (approach 2 & 3) based on vegetation parameters. The vegetation parameters however are themselves subject to large uncertainty. Shadowing on the vegetation canopy can additionally lead to ill-posed vegetation parameter selection. The experiments show the potential of coupled RTM-based quality assessment of high-frequency field measurements but also indicate the need for more accurate vegetation canopy parameter estimates and a more sophisticated optimization process to avoid the effects of ill-posedness.

Contents

List of Figures

List of Tables

Nomenclature and Abbreviations

ARTMO	Automated Radiative Transfer Models Operator
BOA	Bottom of Atmosphere
CAB	Chlorophyll A + B
Cal/Val	Calibration and Validation
CCA	Carotenoid
DESIS	DLR Earth Sensing Imaging Spectrometer
DLR	German Aerospace Center
EnMAP	Environmental Mapping and Analysis Program
E_s^0	extraterrestrial solar irradiance
ESA	European Space Agency
E^{TOC}	TOC Irradiance
FLEX	Fluorescence Explorer
FloX	Fluorescence Box
GGE	Google Earth Engine
HISUI	Hyperspectral Imager Suite
LAI	Leaf Area Index
libRadtran	library for Radiative Transfer
L^{TOC}	TOC Radiance
LUT	Look-Up-Table
MODTRAN	MODerate resolution atmospheric TRANsmission
NASA	National Aeronautics and Space Administration, U.S.A.
θ_s	zenith angle of the sun rays
PRISMA	PRecursore IperSpettrale della Missione Applicativa
RadCalNet	Radiation Calibration Network
r_{dd}	spatially filtered bi-hemispherical reflectance (BHR) of the surroundings
ρ_{dd}	spherical albedo of the atmosphere
r_{do}	hemispheric-directional reflectance factor (HDRF) of the target
RMSE:	Root Mean Squared Error
RMSRE:	Root Mean Squared Relative Error
r_{sd}	spatially filtered directional-hemispherical reflectance (DHR)
r_{so}	bi-directional reflectance factor (BRF) of the target
RTM:	Radiative Transfer Model

SCOPE:	Soil Canopy Observation of Photosynthesis and Energy Fluxes Model
SD	Standard Deviation
SHALOM:	Spaceborne Hyperspectral Applicative Land and Ocean Mission
TOA:	Top of Atmosphere
TOC:	Top of Canopy
τ_{sd}	the diffuse transmittance of the atmosphere for sunlight
τ_{ss}	direct transmittance of the atmosphere for sunlight

1 Introduction

Climate change is affecting global vegetation dynamics through rising temperatures, changing precipitation patterns and increasing solar radiation in general (Afuye et al., 2022; Pricope et al., 2013; Walther, 2010; Wang et al., 2018). Photosynthesis in vegetation is the primary source of energy for life on Earth and results in CO2 uptake, making vegetation monitoring very important in the context of climate change. (Craggs, 2016; Guanter et al., 2014). Satellite remote sensing is a powerful tool to assess vegetation dynamics from local to global scale (Frappart et al., 2020). Multi-spectral images are used to derive a range of spectral vegetation indexes like the normalized difference vegetation index or the enhanced vegetation index and many more (Frappart et al., 2020) which are indicators of photosynthetic activity (Kawabata et al., 2010; Zhou et al., 2001) and productivity (Wang et al., 2010).

Current space-borne imaging spectroscopy systems like the German Aerospace Center (DLR) Earth Sensing Imaging Spectrometer (DESIS) (Eckardt et al., 2015), the Italian PRecursore IperSpettrale della Missione Applicativa (PRISMA) (Candela et al., 2016), the Japanese Hyperspectral Imager Suite (HISUI) (Iwasaki et al., 2011), the German Environmental Mapping and Analysis Program (EnMAP) (Guanter et al., 2015) and upcoming missions such as the European Space Agency's FLuorescence EXplorer (FLEX) (Drusch et al., 2017) or the Space-borne Hyperspectral Applicative Land and Ocean Mission (SHALOM), a cooperation between the Italian and Israelian space agency (Feingersh and Dor, 2015), will not only increase data availability and quality but also extend established spectroscopy-based remote sensing approaches for vegetation monitoring with the measurement of the full chlorophyll fluorescence spectrum emitted by the vegetation (Mohammed et al., 2019).

Spectroscopy offers many possibilities in earth observation. However, spectrometric measurements are also among the most unreliable of all physical measurements (Kostkowski, 1997). Three major sources of error are: (1) the multidimensionality of the measurements, which makes it impossible to look at each measurement individually; (2) the instability e.g. smile and frown of the measuring instruments as well as the methods of their spectral-, geometric- and radiometric calibration; (3) that methods of reducing measurement errors due to the multidimensionality and instability are not widely spread (Schaepman et al., 2002). Further influencing factors include the atmospheric state (Thompson et al., 2019), possible degradation of the sensor (Liu et al., 2020; Nassar et al., 2018; Wang et al., 2012) and many more which cannot yet be properly estimated or corrected for (Curran and Hay, 1986; Hank et al., 2019; Malenovský et al., 2019; Schaepman et al., 2002)

Systematic calibration and uncertainty assessments are of utmost importance for all satellite missions. Calibration and Validation (Cal/Val) activities in the context of imaging spectroscopy have been identified as a key requirement to address important scientific and environmental management objectives worth building a joint working group between the National Aeronautics and Space Administration, U.S.A. (NASA) and the European Space Agency (ESA) (Boccia and Adams, 2021).

The Radiation Calibration Network (RadCalNet) represents another push towards long-term publicly available Cal/Val data based on the cooperation of European organizations. RadCalNet consists of four automated measurement sites in mostly non-vegetated semi-arid regions providing a time-series of in-situ measurements (Bouvet et al., 2019). The three main approaches to space-borne spectroscopy measurement Cal/Val are on-board calibration, the comparison to in-situ measurements and the comparison to space-borne measurements from other missions. In contrast to the larger satellites which are commonly equipped with on-board calibration systems, the rise of smaller satellites without on-board calibration systems will increase the demand and importance of Cal/Val data even more (Sterckx et al., 2020).

DESIS launched in 2018 has been calibrated and validated in orbit using spectrally homogeneous RadCalNet sites as well as by cross-calibration with Landsat-8 and Sentinel-2 scenes. Due to the lack of publicly available Top of Atmosphere (TOA) radiometric reference measurements, Bottom of Atmosphere (BOA) reflectance measurements were upscaled to TOA reflectance and converted to TOA radiance to be comparable to DESIS radiance measurements (Alonso et al., 2019). Cross calibration with other well-calibrated satellites is the second well-established approach applied to validate DESIS measurements (Li et al., 2017; Markham et al., 2014; Odorico et al., 2013; Shrestha et al., 2021). Bright, near-simultaneous nadir acquisitions between DESIS and Landsat-8 or Sentinel-2 over pseudo-invariant sites are preferred to minimize the influence of the atmosphere and geometric properties. As Landsat-8 and Sentinel-2 are only multispectral sensors DESIS measurements need to be integrated to match the spectral resolution (Alonso et al., 2019). Even though being a well-established method cross-validation of hyperspectral data with multispectral data forcibly results in loss of information. Validation with RadCalNet is limited by the sparse availability of measurement sites and the spectral resolution of 10 nm compared to 2.5 nm of DESIS full spectral resolution (Alonso et al., 2019).

Measurements from PRISMA which is in orbit since March 2019 have been assessed over rural areas (Cogliati et al., 2021) and a wide range of water types (Giardino et al., 2020). In-situ, as well as airborne reflectance measurements, were collected over different landcover classes and propagated to TOA radiance using the MODerate resolution atmospheric TRANsmission (MODTRAN) RTM to compare to the satellite observations. The validity of this approach however is limited to similar land cover classes and needs to be redone for other land cover classes like snow, deserts or urban areas (Cogliati et al., 2021). Combining in-situ with airborne validation measurements allows the assessment of measurement quality at different scales. This approach is however not suitable for recurring measurement validation due to the high cost of airborne measurements. PRISMA water body radiance measurement quality has been assessed using autonomous in-situ radiometers and Sentinel-2 observations at six measurement sites and nine measurement times. In-situ water reflectance measurements were propagated by radiative transfer modelling to TOA radiance compatible with the PRISMA measurements. To fully characterize the on-orbit calibration of the PRISMA sensor more

match-ups between PRISMA observation, in-situ measurement and Sentinel-2 observation are needed (Giardino et al., 2020).

Measurements from EnMap launched in April 2022 are being validated following similar approaches as DESIS and PRISMA. In-situ data from Cal/Val sites and cross-validation with other satellites are applied. Being the latest of the three presented spaceborne spectrometers EnMap benefits from the available data from DESIS and PRISMA for validation purposes (Brell et al., 2021).

The two main approaches to space-borne spectroscopy measurement validation (besides on-board validation) are the comparison to in-situ measurements or other satellite data. Regardless of the origin of the data, quality must be ensured. This brings up the problem that the validation data can suffer from the same problems as the products to be validated. Even though field spectroscopy is increasingly used in support of airborne and spaceborne calibration applications, the interaction between light and surface remains complex. Therefore, cross-validation between in situ and airborne spectroscopy measurements has been performed in studies to validate the in situ measurements (Hueni et al., 2017).

The University of Zurich maintains multiple Fluorescence Box (FloX) sites which provide time-series of in-situ spectrometer measurements with the high temporal and spectral resolution needed for Cal/Val applications. The quality of the measurements however is not known and there exists no readily available system to validate them consistently. A new validation approach, independent of additional simultaneous measurements, is needed as installing additional measurement devices on the same site or conducting regular airborne measurements is costly and does not solve the inherent problems with the data.

I propose an approach that simulates in-situ spectrometer measurements by coupling two radiative transfer models (RTM) to compare to the measurements. To achieve accurate radiance simulations, I need to model the transmission of the light through the atmosphere, account for the fraction of light reflected on the surface and model the path back up to the sensor. The coupling of RTMs allows the usage of dedicated RTMs optimized for one specific sphere respectively (atmospheric effects: library for Radiative Transfer (libRadtran), vegetation effects: Soil Canopy Observation of Photosynthesis and Energy Fluxes Model (SCOPE)) to account for the combined effect (Mayer and Kylling, 2005; Van Der Tol et al., 2009).

The idea of coupling RTMs has been applied in previous studies. The most common application so far however was the retrieval of vegetation parameters by model inversion. (Atzberger, 2004; Cui et al., 2020; Kattenborn et al., 2018; Koetz et al., 2006; Laurent et al., 2013, 2011; Lauvernet et al., 2008; Quan et al., 2015; Verhoef and Bach, 2003).

This study aims to develop and evaluate model-based approaches for in-situ spectrometer uncertainty assessment. Three approaches with different complexity and computational demand for simulating in-

situ spectrometric measurements are presented. All approaches are based on libRadtran (Mayer and Kylling, 2005) and SCOPE (Van Der Tol et al., 2009; Yang et al., 2021) and applied to measurements from the FloX spectrometer installed on the Laegeren research site (JB-Hyperspectral Devices UG, 2019; Sutter and Waldner, 2019). The correspondence or the fit between simulation and measurement is subsequently assessed in terms of Root Mean Squared Error (RMSE) and Root Mean Squared Relative Error (RMSRE).

2 Data and Methods

A range of modelling tools as well as in-situ measurement data is needed to build an approach for in-situ spectrometer measurement validation based on RTM modelling. The following section is going to introduce the data and tools used as well as the workflow of the three validation approaches built.

2.1 Study Site

The study site providing the in-situ measurements needed for this work was chosen based on the availability of high temporal- and high spectral resolution data. A spectrometer at the Laegeren research site provides the required time-series of measurements and is directed on a single tree which was suspected to facilitate vegetation modelling. The site is situated at N 47° 28′, 49″ and E 8° 21′, 05″ 682 m above sea level on the south-facing side of the Laegeren mountain, approximately 15 km northwest of Zurich, Switzerland (Figure 1). The southern slope of the Laegeren marks the boundary of the Swiss Plateau which is bordered by the Jura and the Alps. A 45-m-tall tower, originally designed and built as part of the Swiss air quality monitoring network in 1986, provides micrometeorological data. The vegetation around the tower is dominated by beech (Fagus sylvatica L.) which includes the tree in the field of view of the FloX (Eugster et al., 2007). The growing season lasts from 170 to 190 days. The surface cover mainly consists of bare soil, boulders and litter with a sparse understory dominated by herbs and shrubs. The average canopy height was 24.9 m in 2020 with a stem density of 270 stems per ha (Morsdorf et al., 2020; Sutter and Waldner, 2019).

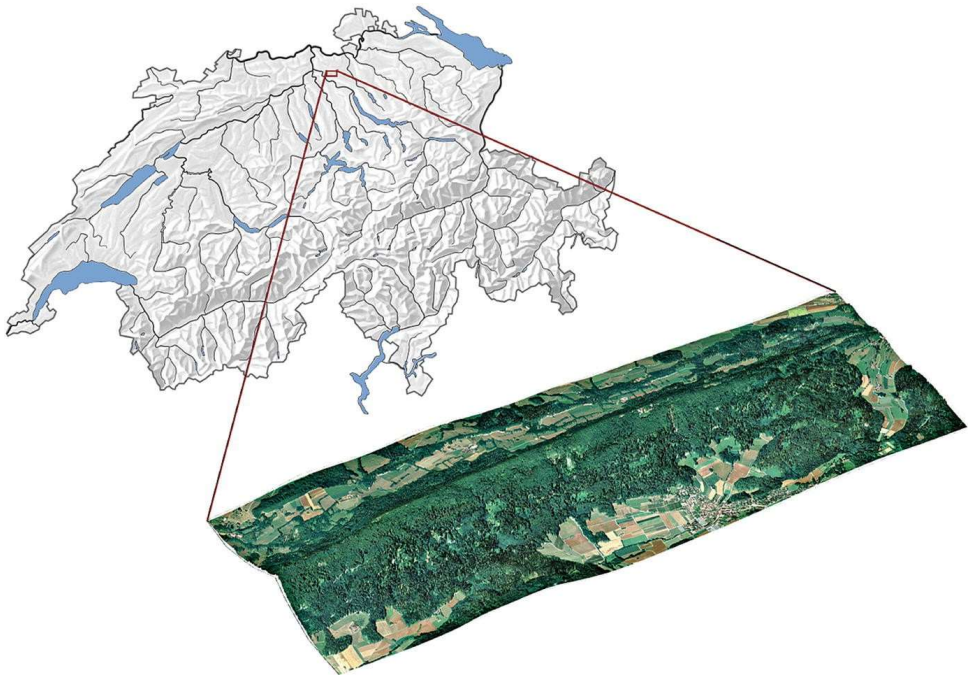

Figure 1: Location and aerial view of the laegeren within Switzerland. (Morsdorf et al., 2020, pp. 87)

2.2 Radiometric Data

The spectrometric measurements used in this thesis were acquired by a FloX system installed on top of the tower on the Laegeren research site. The FloX is designed to passively measure high-frequency spectral data whilst being exposed to the elements (JB-Hyperspectral Devices UG, 2019). Figure 2 depicts the measurement setup.

Two spectrometers are mounted inside the FloX housing each measuring the downwelling irradiance and the upwelling radiance. Based on these measurements the reflectance is calculated (JB-Hyperspectral Devices UG, 2019).

The data used were acquired between 2021/06/10 and 2021/11/10. The dataset contains a total number of 64'149 measurements of irradiance and radiance, and reflectance estimates from the FULL sensor (see Table 1).

Table 1: Sensor specification of the two spectrometer installed in the fluorescence box (JB-Hyperspectral Devices UG, 2019).

	FLUO	FULL
Wavelength range	650 nm to 800 nm	400 nm to 950 nm
Spectral Sampling Interval	~0.17 nm	~0.65 nm
Spectral resolution	~0.3 nm	~1.5 nm
Field Of View	~180° downwelling irradiance, ~20° upwelling radiance	~180° downwelling irradiance ~20° upwelling radiance
Signal-to-noise ratio	1000	250
Quick measurements	20 seconds in bright sunshine, 60 seconds in overcast conditions, Both measurements are taken in one cycle	

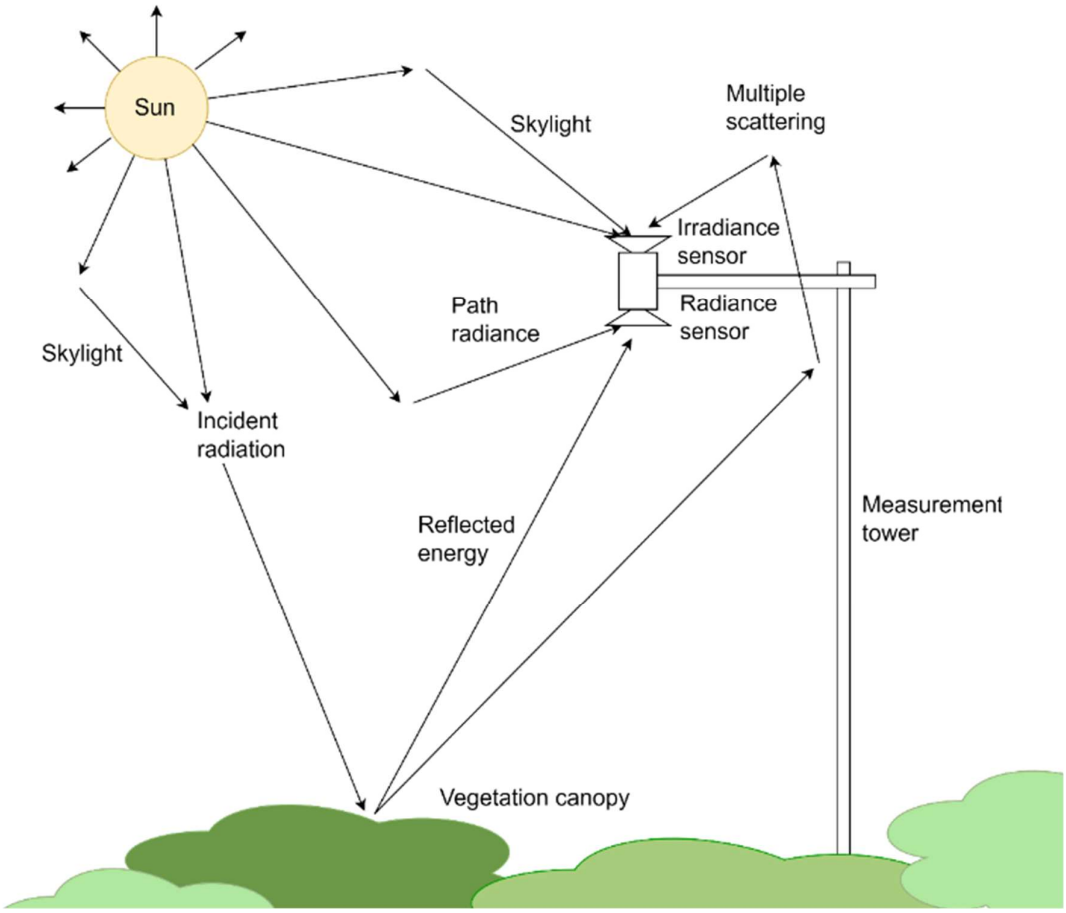

Figure 2: Sketch of the measurement setup and the different radiation paths that contribute to the measured irradiance and radiance signal. Adapted from (Lillesand et al., 2015, pp. 23)

2.3 Radiative Transfer Modelling

To model irradiance and especially radiance at the Top Of the Canopy (TOC) the interactions between incoming radiation and the atmosphere as well as with the vegetation canopy need to be considered (see Figure 2). The top of canopy irradiance E^{TOC} can be approximated according to (Damm et al., 2011) as:

$$E^{TOC} = \left[\tau_{ss} + \frac{\tau_{sd}+\tau_{ss}\overline{r_{sd}}\rho_{dd}}{1-\overline{r_{dd}}\rho_{dd}}\right]\frac{E_s^0 cos\theta_s}{\pi} \quad (1.1)$$

where τ_{ss} is the direct transmittance and τ_{sd} is the diffuse transmittance of the atmosphere for sunlight. r_{sd} represents the spatially filtered directional-hemispherical reflectance. r_{dd} is the spatially filtered bi-hemispherical reflectance of the surroundings. ρ_{dd} corresponds to the spherical albedo of the atmosphere. E_s^0 is the extraterrestrial solar irradiance and θ_s the zenith angle of the sun rays.

Top of canopy radiance L^{TOC} respectively can be approximated according to (Damm et al., 2011) as:

$$L^{TOC} = \left[\tau_{ss}r_{so} + \frac{\tau_{sd} + \tau_{ss}\overline{r_{sd}}\rho_{dd}}{1 - \overline{r_{dd}}\rho_{dd}}r_{do}\right]\frac{E_s^0 cos\theta_s}{\pi} \quad (1.2)$$

where r_{so} is the bi-directional reflectance factor of the target and r_{do} is the hemispheric-directional reflectance factor of the target.

The main difference between irradiance and radiance as shown in equations 1.1 and 1.2 is the multiplication with the reflectance terms of the target (r_{so} and r_{do}) of the latter. Radiance is therefore directly linked to the reflectance of the target. Irradiance is influenced by the reflectance of the target and surrounding area via the spherical albedo of the atmosphere. Irradiance measurements and simulations are therefore also dependent on the reflectance of the target and surroundings but not as sensitive as radiance measurements or simulations.

To account for the interaction with the atmosphere and the fraction of light reflected on the vegetation canopy approximations of the atmospheric transmission and the reflectance spectrum are needed. The transmission through the atmosphere is modelled in all approaches (Table 2). The reflectance spectrum applied by approach 1 however is drawn from the measurements themselves resulting in a simplified, less computationally demanding setup. Approach 2 and approach 3, with approach 3 being a refinement of approach 2, model the reflectance spectrum based on vegetation traits for higher independency from the measurements to be validated. Two individual RTMs, each accountable for one sphere (atmosphere or biosphere), are used and coupled to simulate the measurements and account for the effects in the respective spheres.

Table 2: Overview of the tools and data used to estimate the effects of the atmosphere (Atmospheric transfer function) and the effect of the biosphere (Reflectance spectrum) on the top of canopy signal. Colour-coding: beige: model-based approximation, blue: empirical approximation.

	Approach 1	Approaches 2 & 3
Atmospheric transfer function	libRadtran	libRadtran
Reflectance spectrum	Measurement-based	SCOPE

2.3.1 Overview of Approaches

Consideration of the trade-off between computational effort and dependence on the measurements to be validated led to two main approaches and one further development thereof to model irradiance and radiance. All approaches are based on the assumption that irradiance measurements are less uncertain (equation 1.1 & 1.2) and estimate the atmospheric parameters by iteratively optimizing irradiance. This first step allows checking if irradiance can be reproduced at all. In the second step, radiance is modelled which requires a more accurate reflectance estimation. Two main strategies to estimate reflectance and a further development thereof lead to the three approaches presented in detail below. The underlying motivation of the three strategies however is as follows. First strategy: by using reflectance from the measurements the performance and consistency of the radiance measurements can be assessed directly. Second strategy: by simulating reflectance using vegetation parameters it is possible to check if radiance can be reproduced at all. The higher level of independence from the measurements additionally allows for assessing the correspondence between irradiance and radiance measurement. Third strategy: by using a Look-Up-Table (LUT) of reflectance simulations the influence of using fewer simulations resulting in lower computation times can be assessed. The next paragraphs introduce these approaches in detail.

Approach 1 "FloX-based reflectance" determines the reflectance as the ratio of radiance to irradiance measurements around 13:00. The apparent reflectance is suspected to be closest to the true reflectance at noon to early afternoon as the high sun position should lead to minimal shading (see Figure 4 showing highest radiance in relation to irradiance at roughly 13:00). To provide a more stable signal the reflectance spectra from 12:45 to 13:15 are averaged before being used as input to libRadtran. Using the reflectance spectrum of the FloX makes the coupling of libRadtran with SCOPE obsolete and decreases the number of simulations compared to more advanced approaches relying on SCOPE simulations for the reflectance spectrum. Irradiance and radiance signals are simulated solely by libRadtran and the best fit is determined using RMSE minimization between simulation and closest measurement.

Given date and time, the model checks if a reflectance file is already existing. Otherwise, the reflectance file for libRadtran is calculated and saved so it does not have to be recalculated in a future run. Irradiance is then simulated for all input combinations of aerosols and water cloud optical depth. The best

simulation(s) are determined and the corresponding values of aerosols and water cloud optical depth are saved. Radiance can be simulated by just one run per measurement given date and time as well as the previously determined optimal parameters of aerosol and water cloud optical depth. Even if this is computationally efficient, the high degree of dependence on the measurements is problematic considering the approach is designed to validate the same data.

Approach 2 the "Literature-based parametrization" was designed to work more independently from the measurements. For higher independence from FloX reflectance estimates, we refer to SCOPE simulations based on vegetation parameters to provide a wavelength-dependent reflectance spectrum which is used as albedo in libRadtran.

In the first step, the composition of the atmosphere is approximated by iterating over the predefined range of values of atmospheric properties in the attempt to model irradiance. The composition of the vegetation is left to default except for parameters relating to the time and general setup geometry. These values however are kept constant over iterative runs of altering the atmospheric composition. Inputs to libRadtran are provided by the input string which is adjusted for every successive run of libRadtran. The best fit of the simulation is determined using RMSE minimization between simulation and observation. The atmosphere parameters of the irradiance simulation with the smallest RMSE are then forwarded to the radiance simulation.

In the second step, the radiance simulation is optimized by using the atmospheric composition determined in the first step and iterating over every possible combination of biophysical properties within the given range. The influence of the biophysical properties is modelled with SCOPE and evident in the resulting reflectance file. The MATLAB-based SCOPE model gets called from within Python using the MATLAB ENGINE API (Mathworks, 2021). Altering the input values of the individual runs is achieved by adapting the "Input_data_default.csv" file in the SCOPE folder. Upon completion of all radiance simulations, the best fit is again determined using RMSE minimization. Due to the large number of runs needed approach 2 can however result in high computation times or in low parameter sampling density and thus poorly fitting simulations.

Approach 3 the "LUT-based parametrization" is built upon approach 2 and designed to mitigate the computational burden of the literature-based parametrization approach. A SCOPE model inversion was built to simulate reflectance, compare the simulations to FloX reflectance estimates and save the vegetation parameters that did lead to the best fitting simulations to a LUT. The date-specific estimation of vegetation parameters allows a narrower, more densely sampled parameter range in the following radiance simulation. The model inversion is best run over the whole period of interest focusing on days with near-perfect irradiance to generate a timeline of vegetation parameters. Days without clouds lead to less interaction with the atmosphere and are found by plotting irradiance at one wavelength (e.g. 600 nm) over a day. Given a sunny day, the resulting curve is a smooth parabola with its maximum around

noon. A total of 26 days with near-perfect irradiance were found and simulated over our investigated period.

Atmospheric parameters are again optimized by RMSE minimization between simulation and measurement. The LUT is then used to retrieve temporally dependent vegetation parameter estimates for the radiance simulations. The model chooses the LUT entry closest to the input time, retrieves the vegetation parameters and runs coupled SCOPE-libRadtran radiance simulations for a tighter range around the retrieved values. The best-fitting radiance simulation is found using RMSE minimization. The third approach allows faster computing times or higher parameter sampling density once the LUT is calculated.

2.3.2 Atmosphere Model and Parametrization

libRadtran is used in the presented approaches to model the transmission of radiation through the atmosphere. The RTM included in libRadtran is designed to estimate the radiation field for given atmospheric and surface conditions (Mayer and Kylling, 2005). libRadtran, in contrast to other in remote sensing more widespread RTMs like MODTRAN (Guanter et al., 2009), is open source which allows everyone to adapt or further develop the approaches presented in this thesis.

Uvspec is libRadtran's main tool. The user can choose between ten radiative transfer equation solvers and specify the composition of the atmosphere in detail (Mayer et al., 2017; Mayer and Kylling, 2005). The simulations in this thesis are based on the widely used DIScrete Ordinante Radiative Transfer, solver short DISTORT, code (Mayer et al., 2017; Stamnes et al., 1988).

The atmosphere interacts with the radiation that passes through it in two ways. First, it reduces the amount of radiation that illuminates the ground and is reflected from the ground by scattering and absorption. Second, it increases the measured signal by adding scattered extraneous radiation, acting as a reflector (Lillesand et al., 2015). Aerosols and water cloud optical depth were found to have the greatest impact on irradiance (Al Asmar et al., 2021). Reasonable ranges for the parameters at the Laegeren test site were found based on literature and experience gained during the process (ranges see Table 3). The aerosol type below 2 km is set to rural assuming high air quality outside of major cities in Switzerland.

Table 3: Parameter ranges used in the simulations as an approximation of the atmospheric conditions. The library of Radiative transfer (libRadtran) parameter "aerosol_modify tau set" sets the aerosol content in the atmosphere in [g/m^3] and "wc_modify tau550 set" sets the water cloud optical thickness at 550 nm in [g/m^3] for the libRadtran simulation based on the values provided. The parameter value ranges were defined according to literature and experience gained during the process (Al Asmar et al., 2021; Mayer and Kylling, 2005).

Parameter name libRadtran	Min	Max	Step size
aerosol_modify tau set [g/m^3]	0	2.3	0.2
wc_modify tau550 set [g/m^3]	0	8	1

2.3.3 Vegetation Model and Parametrization

SCOPE is used to estimate the spectral reflectance of the surface in approaches 2 and 3 based on vegetation traits and auxiliary data. SCOPE was developed in MATLAB and simulates the radiative transfer in the soil, leaves and vegetation canopies considering photosynthesis and non-radiative heat dissipation (Van Der Tol et al., 2009; Yang et al., 2021). A large range of outputs can be produced but for this project, only the TOC reflectance in viewing direction is used. Please note that in contrast to equation 1.2 applying six individual reflectance and albedo terms (r_{so}, r_{do}, r_{sd}, r_{dd} ρ_{so} and ρ_{dd}), only one reflectance output of SCOPE is passed on to the libRadtran simulation. Experiments providing libRadtran with individual terms were conducted but resulted in lower correspondence between simulation and measurement and were therefore discontinued.

The composition of the vegetation at the study site and time of measurement is not known. Ideally, the parameters would be measured with high temporal resolution in the field but the high effort involved makes it impossible. Knowledge of the composition of the vegetation however is crucial for the estimation of the reflectance spectrum which directly impacts the simulated radiance. Multiple approaches to parametrize the biosphere which do not require field measurements were examined and applied. Additionally, a simplified approach which works independently of vegetation parameterization was developed.

A multitude of different approaches to estimate reasonable ranges for the parameters of the biosphere failed including satellite-derived estimation, plant trait database estimation as well as brute force approaches. Satellite Chlorophyll A+B (CAB) products mainly focus on the oceans, the Google Earth Engine (GGE) data catalogue does not contain any Carotenoid (CCA) products and the highest spatial resolution of Leaf Area Index (LAI) products is with 500 m (Gorelick et al., 2017) too large for any reasonable point estimation. The plant trait database TRY with close to 12 million entries was queried for fagus sylvatica (beech) and the required trait measurements (Kattge et al., 2020). The availability of measurements was too low, spatially dispersed over the whole world and unfortunately temporarily clustered to an extent that seasonal patterns were no longer reconstructable. In addition to the sparse availability of parameter measurements for beech trees, the transmissibility within species is highly doubtable as leaf side, leaf age and stress status of the tree were found to superimpose the effect of plant

species on the reflectance spectrum (Mohammed et al., 2000). The seasonal dynamic of overstory and understory LAI was measured at the Laegeren in 2015 indicating LAI between 4 and 6 during the season of investigation (Paul-Limoges, 2017). Even if the measurements were taken on the Laegeren, this does not mean that they come from the same tree that is in the field of view of the FloX. The ranges for the biosphere parameters are therefore largely based on literature, experience gained during the process and deliberately widened to decrease the risk of bad fitting simulation due to too narrow parameter ranges (ranges see: Table 4). The ranges do not claim to be exact or transferable to different locations.

Table 4: Parameter ranges for the simulation of the vegetation canopy using the Soil Canopy Observation of Photosynthesis and Energy Fluxes Model. Parameter value ranges are based on literature and experience (Gitelson et al., 2002; Hosgood et al., 1994; Morley et al., 2020; Paul-Limoges, 2017; Scartazza et al., 2016; Thimonier Rickenmann and Schleppi, 2011).

Parameter name SCOPE	Min	Max	Step size
Leaf chlorophyll concentration [µg/cm2]	30	45	5
Leaf carotenoid concentration [µg/cm2]	5	20	5
Leaf Area Index [m2/m2]	3	15	1

2.3.4 Model Coupling

libRadtran is capable of calculating the atmospheric effects but not optimized to estimate the interaction with the vegetation. Default reflectance spectra are available (Mayer and Kylling, 2005) but not fit for our purpose. SCOPE is well suited to estimate the spectral reflectance at the study site as the vegetation in the field of view is known. Accurate simulations, therefore, require a coupled model where libRadtran is provided with SCOPE-based estimations of the spectral reflectance or albedo.

SCOPE and libRadtran are coupled by adapting the SCOPE reflectance output to the format of the libRadtran albedo files and providing it as input to libRadtran.

2.3.5 Model Parallelization

Parameters for the atmosphere (aerosols and water cloud optical depth), biosphere (CAB, CCA and LAI) as well as the point in time (determines illumination geometry) lead to a six-dimensional input space for the coupled model. The high dimensionality of the input space not only causes high computation times but also a huge input sampling space and low sampling density. Low sampling density increases the probability of bad-fitting simulations. The architecture of the coupled model was therefore improved to achieve higher sampling and lower computation time.

To break down the sampling space the optimization process of atmospheric parameters and vegetational parameters was split apart. The sensitivity to reflectance spectrum misspecification is, based on Equations 1.1 and 1.2, smaller for irradiance simulations compared to radiance simulations. The atmospheric parameters are therefore optimized by iterative runs over atmospheric compositions using a single SCOPE reflectance estimation. The SCOPE configuration is left to default except for site and

date-specific inputs (e.g. date, coordinates, altitude, vegetation height, measurement height (Sutter and Waldner, 2019), solar- and viewing zenith angle calculated by pysolar (Zebner et al., 2014)) which are still provided. The atmospheric parameters get fixed to the values of the irradiance simulation with the highest correspondence to the measurement. The atmospheric parameters are then used as input for the radiance simulations which iterate over the combinations of vegetation parameters.

In a second step, the setup of the models was optimized to run in parallel on as many cores as the available system allows. Running the models on a small server with 8 cores based on the multiprocessing library in python ("Process-based parallelism", 2022) helped additionally and made running simulations overnight more convenient. Overall the computing time was reduced by more than 85% compared to the original setup on a local machine.

2.4 Statistical Analysis of Measurement and Simulation

To evaluate the performance of each model, simulations were run on all sunny days of the 154-day measurement period at 1 pm. The time for the simulations was chosen as shading is suspected to be lowest in the early afternoon as Figure 4 shows the largest radiance in relation to irradiance at roughly 13:00. The correspondence between measurement and simulation is determined using the RMSE in the wavelength region between 400 and 800 nm (Despotovic et al., 2016).

The RMSE is defined by

$$RMSE = \sqrt{\frac{1}{n}\sum_{i=1}^{n}(obs_i - sim_i)^2} \tag{2.1}$$

As a more tangible measure of error, the RMSRE is provided additionally and used for the analysis (Despotovic et al., 2016).

The RMSRE is defined by

$$RMSRE = \sqrt{\frac{1}{n}\sum_{i=1}^{n}\left(\frac{obs_i - sim_i}{obs_i}\right)^2} \tag{2.2}$$

where obs are the observations of the FloX, sim the simulations to be validated and n the number of wavelengths considered.

3 Results

The performance of the individual models was assessed over the season and over the time of a single day. To do so irradiance and radiance were simulated for every day of the investigated period at 13:00 and at hourly rates on the 2nd of September and compared to the measurements.

3.1 Seasonal and Diurnal Irradiance and Radiance Dynamics

The focus of the analysis was placed on sunny days, as today's models cannot fully compensate for the influence of the weather (Al Asmar et al., 2021). Most outliers in the error measurement time-series are suspected to be caused by weather-related effects. This conjecture is supported by usually very low irradiance and radiance measurements at the time of bad-fitting simulations.

Days with perfect irradiance were identified by visually assessing the curve of the irradiance at 600 nm plotted over the time of the day. If the curve is a smooth parabola with its maximum around noon without any major disruptions in the profile the day is considered perfectly sunny or also clear-sky (Figure 3).

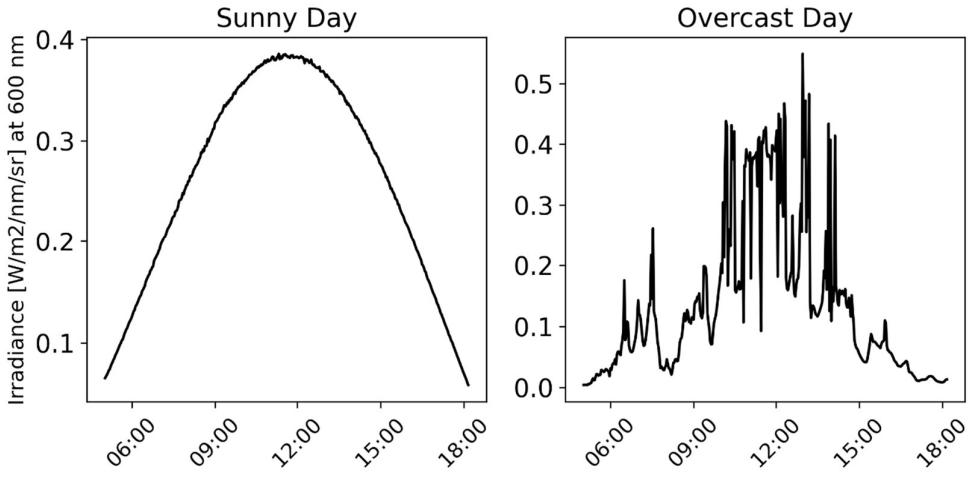

Figure 3: Plot of the irradiance at 600 nm over a sunny day (left) with perfect irradiance and an overcast day (right) with non-perfect irradiance.

Of the 154 days in total, only 8 were found to match the requirements. The irradiance and radiance curves of the selected days are displayed in Figure 4. The radiance signals are less regular showing sharp short-term variation in the measurements. Given the smooth irradiance profile, the sharp changes in the radiance profile must be caused by sudden changes in the reflectance profile. As the composition of the vegetation does not alter at that temporal rate the changes in reflectance are assumed to be induced by illumination effects or shadowing. The effects of shadowing on reflectance cannot be modelled with the current setup and are one of the main reasons for the higher uncertainty of radiance simulations.

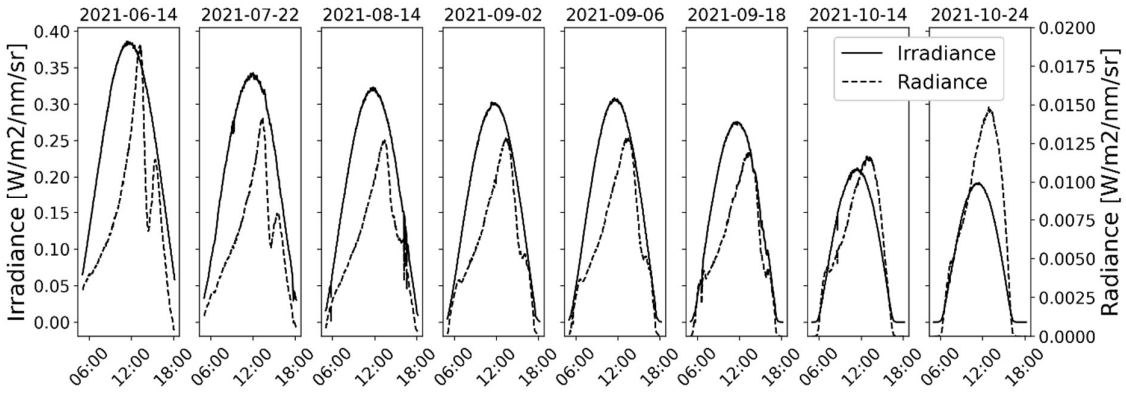

Figure 4: Irradiance and radiance of sunny days from 05:00 to 18:10 at 600 nm. The decline in the magnitude of the signal over the measurement time was expected as a consequence of the seasonal variation in solar irradiance. Y-range for irradiance on the left and for the radiance on the right.

3.1.1 Method Comparison – Seasonal Effects

Irradiance and radiance simulations were run on all sunny days and by all approaches. Figure 5 shows the variation in correspondence between measurement and simulation on days with good-fitting simulations to days with poor-fitting simulations. To visually assess the fit of all simulations consult Figure 12 in the appendix. To make the approaches more comparable, the focus of the analysis was placed on the RMSRE instead of the visual assessment.

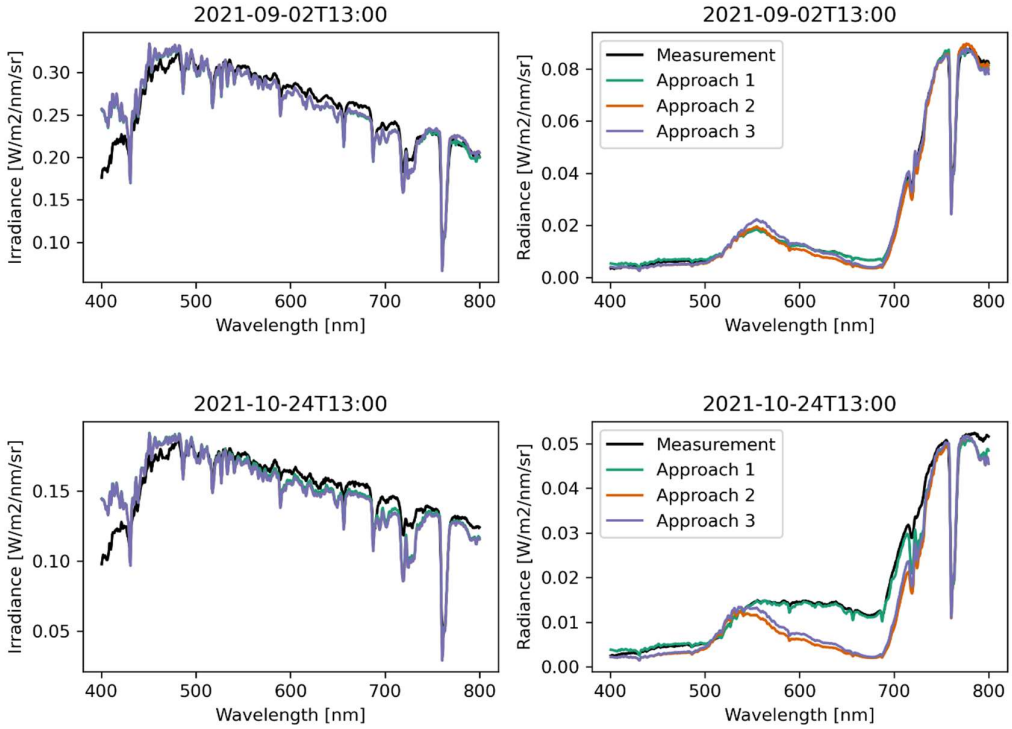

Figure 5: Examples of a day with well-fitting simulations (2021-09-02 upper) and a day with bad-fitting simulations (2021-10-24 lower) with corresponding fluorescence box measurements from the laegeren site.

The mean and median RMSRE for irradiance simulations on sunny days is below 8.5 % for all 3 approaches (Table 5). Approach 1 is marginally lower in RMSRE and Standard Deviation (SD) than approaches 2 & 3. Based on their architecture approaches 2 & 3 result in the same irradiance simulation if given the same parameter range and measurement to optimize - which was the case in this analysis (see Table 3 for applied parameter ranges). The small difference between mean- and median RMSRE as well as the generally small SD can be seen as an indication of model stability.

Radiance simulations have higher RMSRE compared to irradiance simulations independent of the applied approach. Approach 1 results in the lowest RMSRE of ~10 % compared to ~24 % and ~21 % for approaches 2 & 3 respectively. Approach 1 again has a marginally lower mean RMSRE and low SD. Approaches 2 & 3 however show 4 - 5 % lower median RMSRE compared to mean RMSRE and a ten-fold increase in SD compared to Approach 1. These measures suggest lower stability of approaches 2 & 3 in radiance simulations.

Table 5: Summary of Mean, Median and Standard Deviation (SD) of Root Mean Squared Relative Error (RMSRE) for Sunny Irradiance and Radiance Simulations in Percent [%].

	RMSRE on Sunny Days							
	Irradiance				Radiance			
Approach #	1	2	3	Ø	1	2	3	Ø
Mean RMSRE [%]	8.10	8.36	8.36	8.27	10.36	23.81	20.83	18.33
Median RMSRE [%]	8.00	8.29	8.29	8.19	10.70	20.02	16.47	15.52
SD of RMSRE	0.0058	0.0065	0.0065	0.0063	0.0081	0.0924	0.0843	0.0616

Figure 6 (left) displays the temporal distribution of RMSRE for irradiance and shows clearly that approach 1 performs best over the whole period investigated. The range of error is between 7.5% and 10%. The value range of RMSRE of radiance simulations (Figure 6 right) is ~10 to ~45%. Approach 1 yields the lowest RMSRE values, shows low variance and no seasonal pattern. Approaches 2 & 3 yield higher RMSRE values in general, have higher variability and do show a seasonal pattern of increasing RMSRE towards the end of the season. However, RMSRE stays below 25% for all approaches and days except the last two days which result in very high RMSRE estimates for approaches 2 & 3.

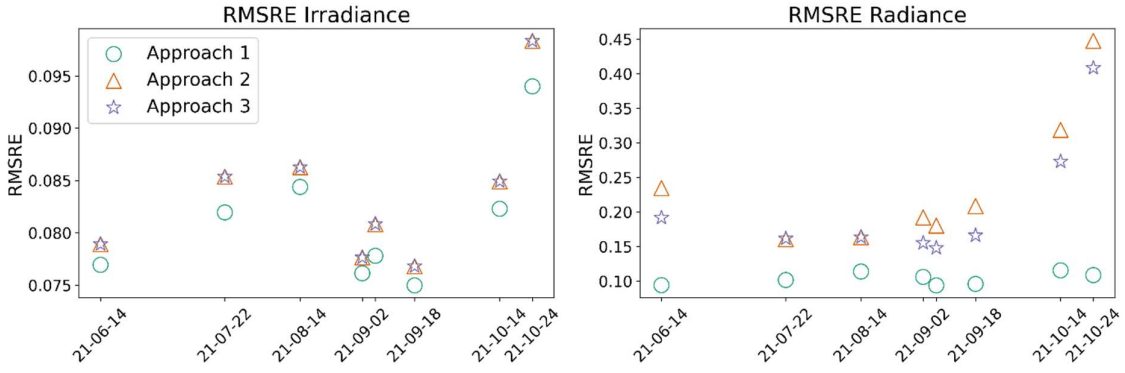

Figure 6: Root Mean Squared Relative Error (RMSRE) between measurement and simulation for all 3 approaches on sunny days from 2021-06-14 to 2021-10-24 for irradiance (left) and radiance (right). Approach 1: green circle, Approach 2: orange triangle, Approach 3: blue/violet star.

3.1.1.1 Input Parameter Distribution

The parameters of the atmosphere (Figure 7 upper) cluster in a limited space of the previously defined parameter range (Table 3). No pattern over the season is apparent. Approach 2 & 3 do again agree on the chosen parameters based on their architecture which can therefore not be seen as two independent approaches converging to the same optimum.

Biosphere parameters are only available for approaches 2 and 3 as approach 1 works independently of a specification of the biosphere. No distinct seasonal pattern is visible. The two approaches did converge in a stable level of 10 µg/cm2 CCA content in the majority of the simulations. Biosphere parameters and radiance simulations in general are not forced to converge by the architecture of the model and therefore indicate agreement in parameter selection by the two models. The CAB content is estimated in a narrow range by both approaches. Approach 3 results in slightly lower CAB values in the second half of the investigated measurement time which could be caused by decreasing CAB content during senescence. The LAI is generally estimated very high at 14 for most simulations by approach 2. The temporal distribution of LAI by approach 3 is parabola shaped with the minimum at 6 right at halftime of the investigated period.

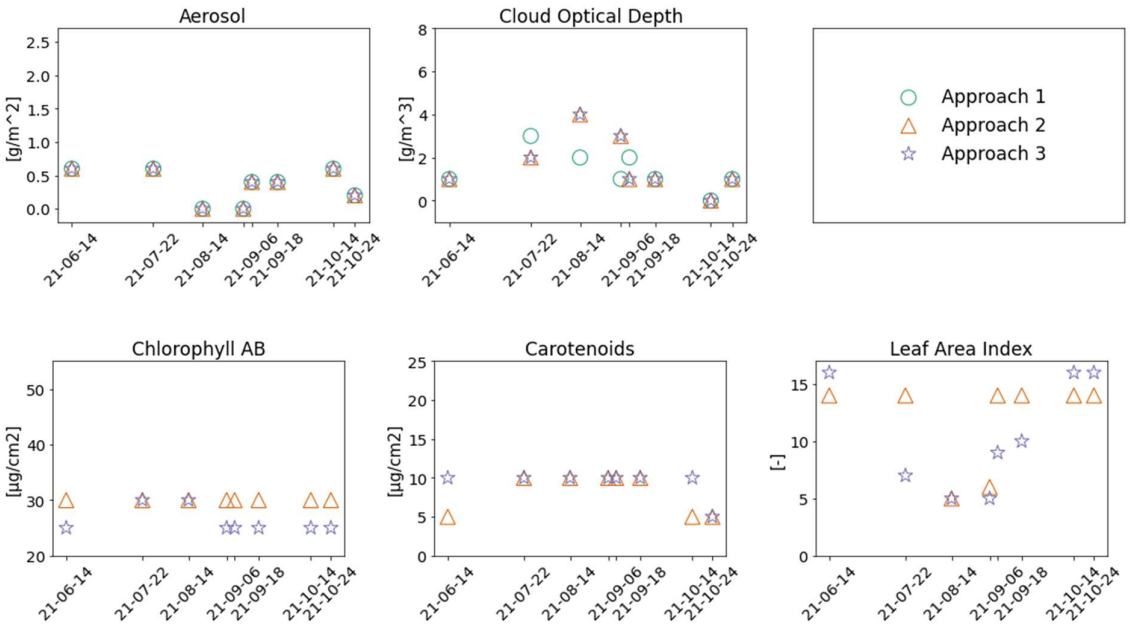

Figure 7: Atmosphere- (upper) und biosphere- (lower) parameter distribution on sunny days. Y-limits are set to the respective parameter range for each atmosphere- and biosphere parameter.

3.1.2 Method Comparison – Diurnal Effects

Hourly simulations by all approaches were run on the 2nd of September 2021. Simulations past 18:00 did result in an RMSRE of 100% as the best simulations dropped heavily below the measurements. The investigated time was therefore limited between 06:00 and 17:00. The simulation fit of selected times can be assessed in Figure 8. For the visual assessment of all simulations consult Figure 13 in the appendix.

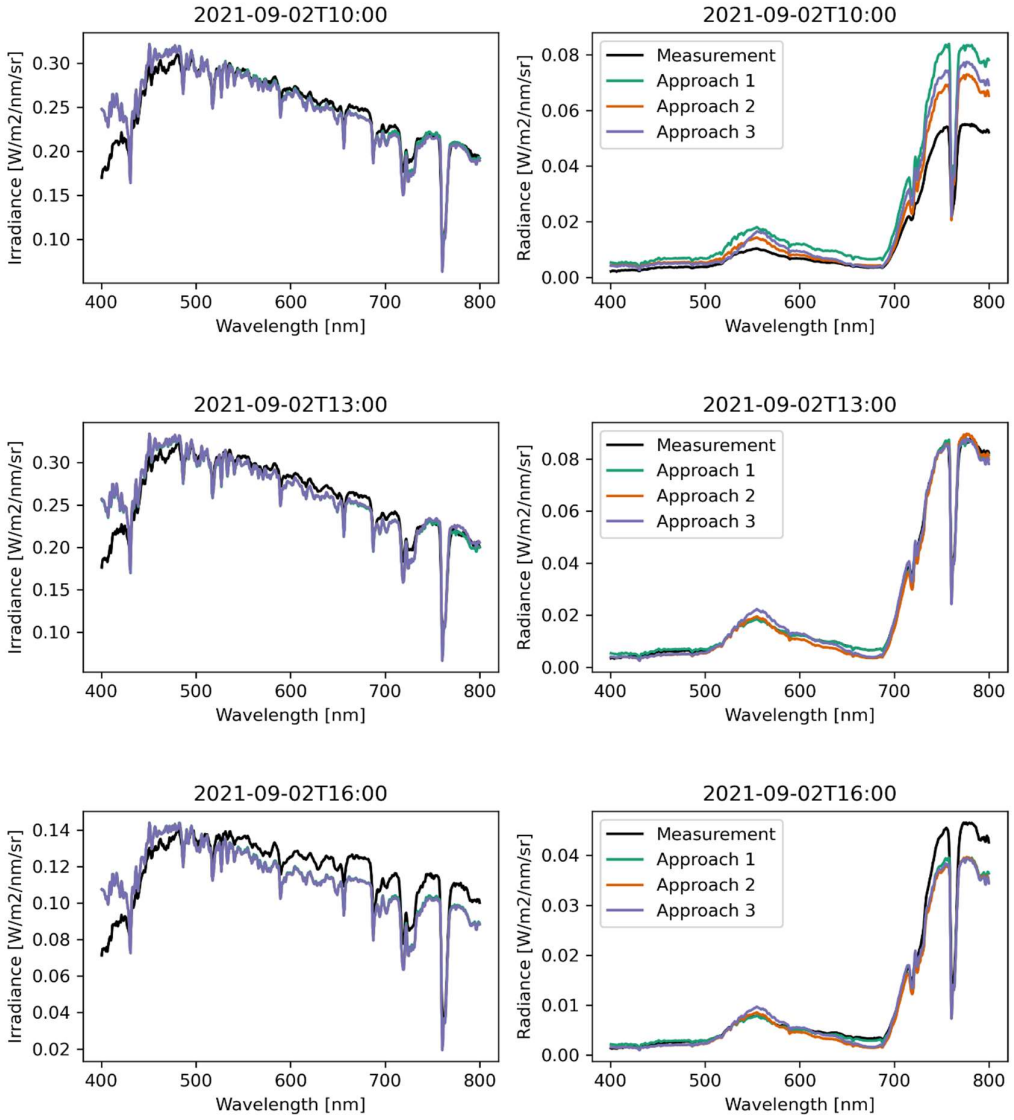

Figure 8: Irradiance (left) and radiance (right) simulations of selected times on the 2nd of September 2021 together with the measurement from 400 nm to 800 nm.

The mean RMSRE of irradiance simulation for all approaches is below 10%. Approach 1 provides simulations with a very slightly lower mean RMSRE compared to approaches 2 and 3 (Table 6).

Radiance simulations did result, independent of the applied approach, in much higher RMSRE values than irradiance simulations. The mean RMSRE for radiance simulations over all approaches (28.83) is

just over three times larger than the mean RMSRE for irradiance simulation over all approaches (9.63). Approach 1 performed worst with an RMSRE of ~38% compared to approaches 2 and 3 with ~24% and 25% respectively. The SD in RMSRE of approach 1 radiance simulations is by far the highest observed indicating large variability between the fit of the simulations and low stability over the day.

Table 6: Mean, Median and Standard Deviation (SD) of Root Mean Squared Relative Error (RMSRE) for irradiance (left) and radiance (right) hourly simulations for all 3 approaches on the 2nd of September 2021 from 06:00 to 17:00.

	RMSRE on the 2nd of September 2021							
	Irradiance				Radiance			
Approach #	1	2	3	ø	1	2	3	ø
Mean RMSRE [%]	9.51	9.69	9.69	9.63	37.81	23.95	24.74	28.83
Median RMSRE [%]	7.79	7.95	7.95	7.90	29.16	23.12	21.58	24.62
SD of RMSRE	0.0332	0.0332	0.0332	0.0332	0.2424	0.0784	0.0835	0.1348

Figure 9 displays the temporal distribution of RMSRE values over the day and the agreement of the three approaches. The temporal distribution of RMSRE values for irradiance simulations is a parabola with a wide bottom around noon. Simulations before 08:00 and after 14:00 have higher RMSRE. All approaches performed about equally.

RMSRE values of radiance simulations peak from around 09:00 to 10:00 depending on the approach. Approach 1 shows higher variance in RMSRE over time compared to approaches 2 and 3 which have a similar temporal pattern but less variance between simulations. The lowest RMSRE values are at 13:00 for approach 1 and at noon for approaches 2 and 3 respectively.

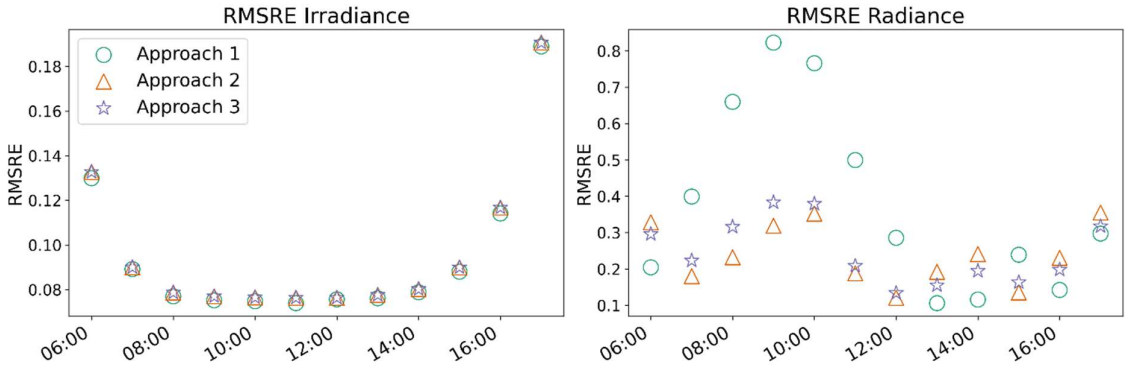

Figure 9: Plot of the Root mean Squared Relative Error (RMSRE) of irradiance (left) and radiance (right) simulations from 06:00 to 17:00 for all 3 approaches on the 2nd of September 2021 over time.

Figure 10 illustrates the temporal parameter distribution of the atmosphere (upper) and the biosphere (lower) within their respective parameter ranges over time.

Optimal aerosol and cloud optical depth values cluster within the lower half of the parameter range. No distinctive pattern is visible. Vegetation parameters are quite stable in the morning but show unrealistically large variation over the whole day.

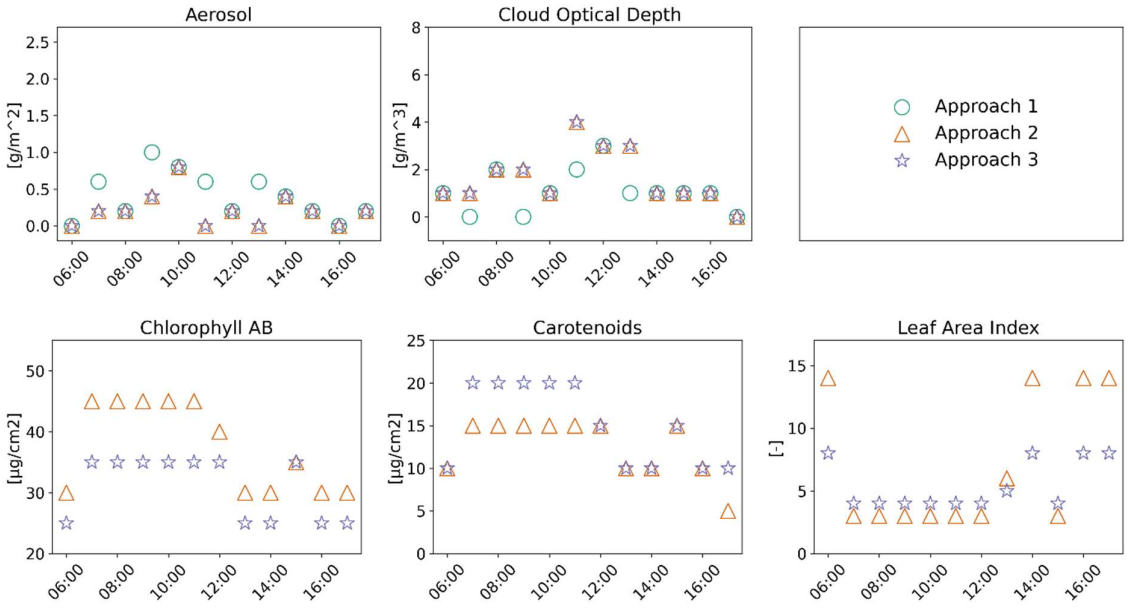

Figure 10: Atmosphere (upper) and biosphere (lower) parameters of optimal hourly simulations on the 2nd September 2021 from 06:00 to 17:00.

4 Discussion

4.1 Correspondence between Simulated and Measured Radiance and Irradiance

4.1.1 Irradiance

Irradiance simulations did generally fit the FloX measurements better in terms of RMSRE compared to radiance simulations. This was expected as misspecification in the reflectance spectrum has a much lower influence on irradiance than on radiance. Irradiance simulations on sunny days were consequently not heavily affected by seasonal senescence and show only a marginal increase of 1% RMSRE on the last date in the investigated period compared to the mean RMSRE over the investigated period. The water cloud optical depth parameter applied in the simulations is the most important parameter to compensate for clouds which have a large impact on irradiance on non-clear-sky days (Al Asmar et al., 2021). Simulations on cloudy days did show, however, that the current setup can only partially compensate for clouds and results in increased RMSRE. Including fractional cloud coverage in irradiance simulations has been proposed to further increase the accuracy of direct irradiance estimates (Al Asmar et al., 2021). Due to the multiplicative increase of model runs needed by iterating additional atmosphere parameters the greatest disadvantage would be the increase in computational demand. The performance of a sensor in real-life applications however usually deteriorates over a prolonged time (Liu et al., 2020; Wang et al., 2012) which makes sensor validation based only on sunny days feasible. If measurement validation on cloudy days is needed the adaption of fractional cloud cover in the model could be beneficial.

Approach 1 performed best for every sampled day in the season at 13:00. The increase in accuracy however is only marginal (0.26%). We do suspect that the difference originates in the reflectance spectra as the transmission through the atmosphere is modelled the same for all methods. Conversely, this implies that modelling the reflectance spectrum with SCOPE only leads to an increase in the mean RMSRE of 0.26% in irradiance simulations at 13:00, compared to using reflectance spectra directly from the measurement. However, based on the daily simulations we are unable to tell whether the SCOPE simulations approach the true reflectance or if the influence of the reflectance spectra is just very low.

The time of the simulation influences the resulting RMSRE. Simulations before 08:00 and past 15:00 result in high RMSRE values reaching 100% already at 18:00. The time of the day surely determines insolation but is accounted for in libRadtran as well as in SCOPE (Mayer et al., 2017; Mayer and Kylling, 2005; Zebner et al., 2014). As the influence of the vegetation canopy and the reflectance spectrum on irradiance simulations is expected to be small we suspect that the underestimation of irradiance in our simulations (Figure 13) and the increase in RMSRE (Figure 9) in the early morning and late afternoon by all approaches to be caused mainly by libRadtran. The effects could however also be caused by the measurement setup.

Approach 1 uses the reflectance spectrum calculated based on the measurements at 13:00 for all times of the day to simplify the model. However, investigations of the apparent reflectance in the measurements (Figure 11 right) show large variation in reflectance over the day in wavelength regions upwards of 725nm due to shading and possibly due to variation in the composition (e.g. leaf water content, stress) or orientation (e.g. leaf angle) of the vegetation (Cipar et al., 2008; Petibon et al., 2021, Alex Damm, Personal Communication 2022). Figure 11 left shows that the variation in the reflectance spectra on sunny days over the season is smaller than the variation over a day.

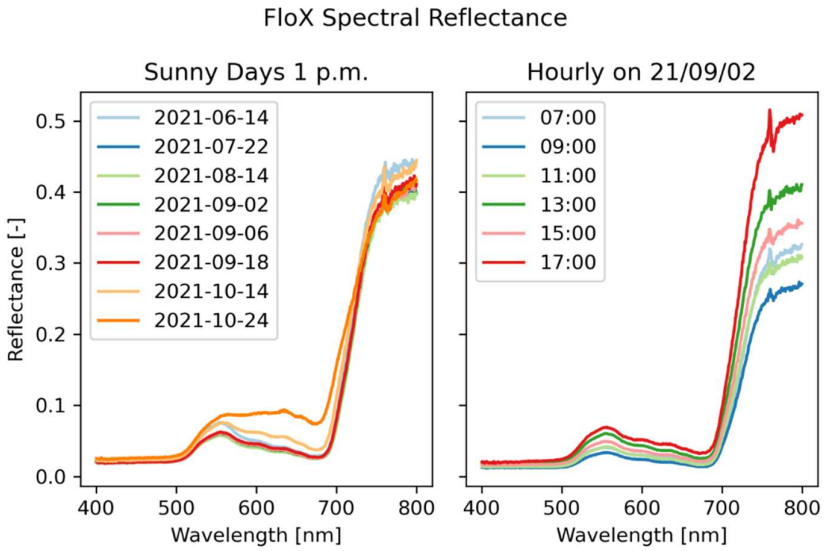

Figure 11: Reflectance spectra from fluorescence box measurements (left) for sunny days at 13:00 and (right) every two hours on the 2nd of September 2021.

Surprisingly approach 1 still performs slightly better than the other approaches even if constantly using the reflectance spectrum at 13:00. As the simulations overall are fitting rather well with a mean RMSRE of below 10% we conclude that the reflectance spectra are not of high importance in irradiance simulations. Additionally, we find that the SCOPE simulations are not capable of fully reconstructing the reflectance as the two approaches which tried to simulate the reflectance at the time of the measurement performed slightly worse than using reflectance from measurements at 13:00. Including additional vegetational parameters may lead to a better fit at the cost of higher computing time.

Generally, it is found that for irradiance simulations, differences in RMSRE between simulations are caused by libRadtran and differences between approaches on the same date are caused by SCOPE. The influence of the reflectance spectra on irradiance is not high enough to make a large difference in performance between the approaches, but it is the only difference between the approaches on the same date and time of the simulation. Additionally, it follows that the choice of the approach does not matter as much as the time and parameter range of the atmosphere parameters.

4.1.2 Radiance

Radiance simulations generally result in higher RMSRE and show higher variation between the approaches. As the transmission through the atmosphere is optimized during irradiance simulation and always run with the same configuration there is not much potential for additional error based on atmospheric transmission except for the path back from the surface to the sensor. The additional path is compensated for by providing measurement height and vegetation height to libRadtran and should not have a large influence. Approach 1 performs by far the best with a mean RMSRE of ~10.5% over sunny days at 13:00 and shows no seasonal pattern compared to 24 % and 21 % with distinct seasonal patterns (Figure 6). The fact that all approaches lead to similar good agreement in irradiance, but approaches 2 and 3 lead to lower agreement in radiance, shows that reflection simulation is problematic Especially simulations towards the end of the season (14th and 24th of November) have high RMSRE with values around 30% and 42% respectively. As approach 1 which is relying on the spectral reflectance from measurements on the respective dates does not suffer from similar effects we conclude that SCOPE-based reflectance simulations do not maintain a constant degree of fit to the true reflectance over the season. This indicates that the parametrization of SCOPE is problematic and needs better ground truth. The outcomes additionally demonstrate the high sensitivity of radiance simulations to reflectance spectra simulation misspecification. The increasing RMSRE towards the end of season is suspected to be caused by a too high CAB value in reflectance simulations which leads to an underestimation of radiance between 550 nm and 700 nm (Figure 12). CAB was expected to decrease during senescence which it only did in approach 3. CAB in approach 2 however was not able to decrease as it was already estimated at the lowest possible value in June. This indicates that the literature-based parameter range estimation is off or that interaction between multiple vegetation parameters leads to unrealistic combinations. Overstory LAI at the laegeren site over the months of interest was measured at between 4 and 6 in 2015 (Paul-Limoges, 2017) which is considerably lower than the simulation estimates of LAI up to 14. As high CAB content reduces reflectance and high LAI increases reflectance one explanation for the unexpectedly high values in both parameters could be the compensation of too high CAB by too high LAI. The origin of the compensatory mechanisms could either be a too high lower limit for CAB but also effects of ill-posedness concerning high LAI generally resulting in good fitting simulations.

Against the simplifying assumption of constant reflectance over the day the apparent reflectance spectrum was found to vary heavily over the time of a day which is not compensated for by approach 1. Approach 1 accordingly results in a very high mean RMSRE of ~38% in simulations over the course of a day. Approaches 2 & 3 allow higher variability in reflectance by either iterating all possible combinations or retrieving the best parametrization from LUT resulting in 25% and 24% mean RMSRE respectively. Interestingly the highest RMSRE of 80% by approach 1 does not occur at marginal times of the day but at 09:00. Measurement-based reflectance estimations (Figure 11) are lowest around 09:00

to 10:00 which could explain the overestimation of reflectance by SCOPE and the resulting overestimation of radiance at 09:00 evident in simulations by all approaches but strongest in approach 1 (Figure 13).

As opposed to irradiance simulations where temporal performance differences are suspected to be caused by libRadtran the same does not hold for radiance simulations. The influence of the reflectance spectrum largely dominates the resulting simulation fit. The current SCOPE configuration is not capable of maintaining the same fit of modelled spectral reflectance over the season or the time of the day. Over the time of a day, however, the reflectance modelling approach provides a better fit resulting in smaller SD between simulations compared to assuming constant reflectance. The cause of the low reflectance at 09:00 (largest RMSRE) is not known but could be caused by shadowing effects. Vegetation parameters were expected to be stable over the span of a day. The results however show variation in the vegetation parameters suspected to be triggered by illumination effects. SCOPE simulations in the current setting are not capable of compensating for shadowing effects directly. The effects of the shadowing are partially compensated by altering vegetation canopy composition. The improvement in the modelled reflectance does therefore not correspond to a more accurate model but compensation of shading effects by vegetation composition.

4.1.3 Challenges and Limitations of this Study

Parameters used in the optimal runs can be retrieved but are ill-posed which is characteristic of model inversions (Laurent et al., 2013). Currently, the simulations are optimized to fit the measured signal by RMSE minimization but do not take into account the likelihood of input combinations. The problem of ill-posedness could be reduced by using a priori information, temporal restraints or Bayesian statistics (Laurent et al., 2011; Lauvernet et al., 2008; Quan et al., 2015).

Especially for radiance simulations more accurate, a priori biosphere parameter knowledge would be beneficial to run simulations with a smaller value range but higher sampling density. Accurate field measurements with high temporal sampling would allow defining smaller ranges around time-based optimal parameters with very high sampling density. However as field measurements are only valid for one location, time-consuming and expensive, Bayesian network-based approaches may be more promising. Bayesian statistics are used to reduce the probabilities of unrealistic combinations by introducing the model's free parameter into their prior joint distribution (Quan et al., 2015). Currently, we suspect that shadowing effects are often compensated by the interplay of CAB and LAI. Allowing only realistic combinations as model input would therefore help to develop a more stable model. The problem of ill-posed parameter selection and large uncertainty of the parameter ranges together with shadowing effects lead to high RMSRE for simulations over the day. To achieve a consistently good fit throughout the day, more a priori knowledge of the vegetation parameters, as well as a more sophisticated optimization process, is needed.

4.1.4 Towards Improved Capacity to Evaluate Accuracy of Field Spectral measurements

The current approaches presented in this work remain limited to clear-sky days with perfect irradiance as clouds cannot be fully compensated for. Whilst irradiance could be modelled through the whole investigated period and over most of the time of the day with good accuracy, radiance measurements showed much higher sensitivity to errors in the reflectance spectrum. The high accuracy of radiance simulations at 13:00 of approach 1 should not blindly be trusted as the simulations are dependent on the measurements we are trying to validate. The suitability of the simulations to validate the measurements overall is hard to assess as we do not have validated nor corrupt measurements to compare to.

We propose to run simulations on sunny days at 13:00 by approaches 2 &3 during a period when the FloX sensor was known to be degraded and compare the resulting RMSRE values to the values obtained in this project. Approach 1, even though delivering the best accuracy over the season at 13:00 is not appropriate for measurement validation due to its heavy dependency on the measurements themselves.

Better a priori parameter estimation and a more sophisticated optimization process are needed to increase the consistency of the parameter estimations which would ensure that simulation fits are not due to chance. To validate all measurements of the FloX in live time more computational power or the use of emulators that approximate RTMs with statistical learning (Rivera et al., 2015; Verrelst et al., 2019, 2017) is needed as the current setup would take more than 24 hours to run simulations for all measurements of a day which makes live validation impossible. The Automated Radiative Transfer Models Operator (ARTMO) emulator toolbox could be used for that task (Verrelst and Rivera, 2021).

5 Conclusion

I conclude that simulated and measured irradiance agree well with a mean RMSRE of below 10% over the season and over the time of the day for all approaches. Radiance simulations resulted, due to the higher sensitivity to canopy reflectance, in a higher RMSRE of ~10 %, ~24 % and ~20% over the season at 13:00 and ~38 %, ~24% and ~25% over the time of the day for the respective approaches. Investigations showed large variation in the estimated reflectance profiles of the measurements over the day caused by shadowing effects which currently cannot fully be compensated for by the model. I conclude that more accurate reflectance spectrum modelling is needed to enable validation of field spectroscopy radiance measurements, e.g. by using better a priori vegetation parameter estimates and a more sophisticated optimization process. Bayesian network approaches would additionally allow to reduce the compensation of shadowing effects by vegetation composition changes and provide more stable simulations. To enable measurement validation on non-clear-sky days the adaption of the cloud fractional cover and possibly additional atmosphere parameter is needed. To meet the increased demand for computational power the use of emulators should be considered as an option to allow more dense parameter sampling with higher computational speed. Finally, I would like to stress the importance of further research on the effect of shadowing and how these effects could be integrated into RTM-based field spectroscopy measurement validation.

Appendix

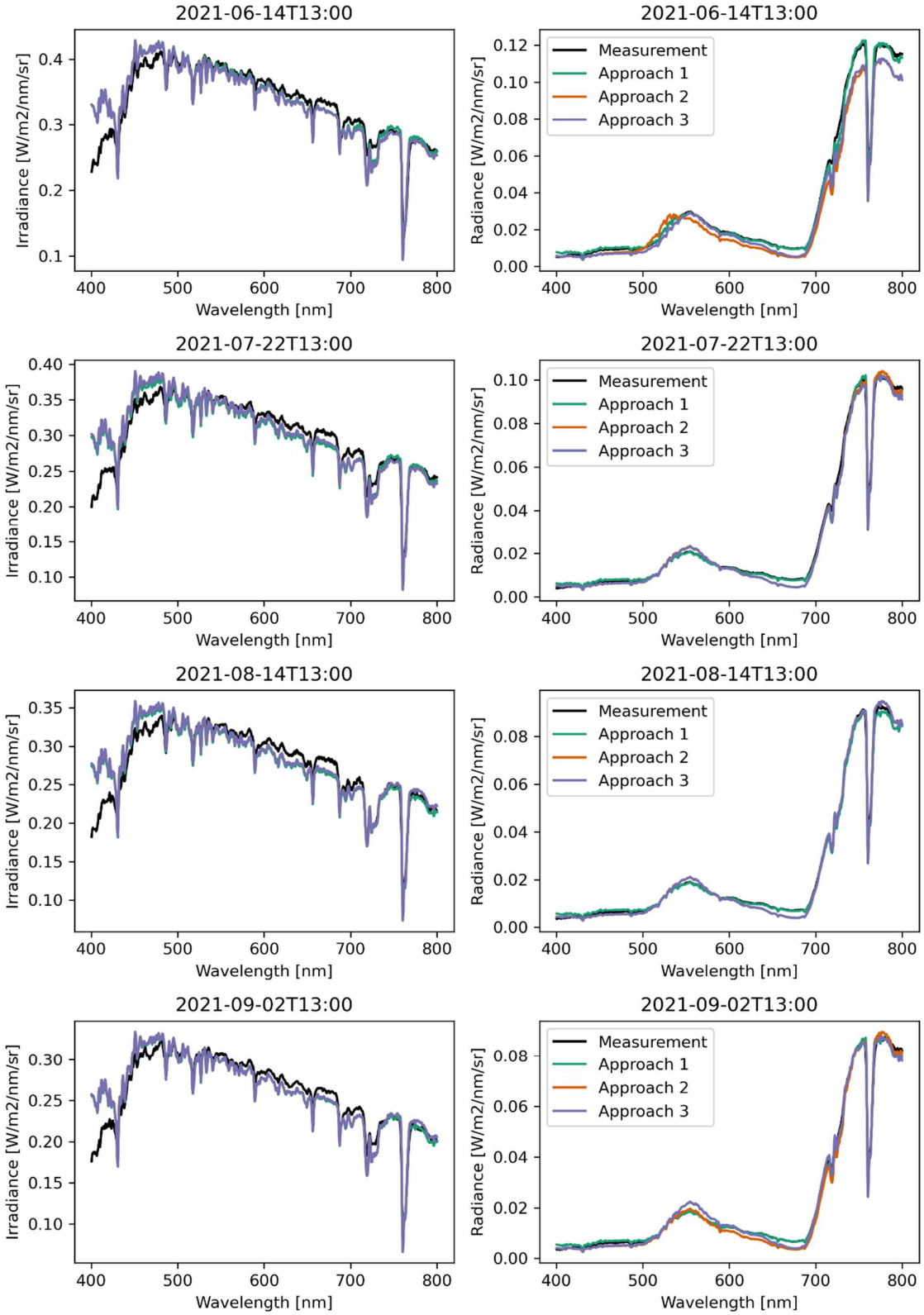
2021-06-14T13:00
Irradiance [W/m2/nm/sr]
Wavelength [nm]
2021-06-14T13:00
Radiance [W/m2/nm/sr]
Measurement
Approach 1
Approach 2
Approach 3
Wavelength [nm]
2021-07-22T13:00
Irradiance [W/m2/nm/sr]
Wavelength [nm]
2021-07-22T13:00
Radiance [W/m2/nm/sr]
Measurement
Approach 1
Approach 2
Approach 3
Wavelength [nm]
2021-08-14T13:00
Irradiance [W/m2/nm/sr]
Wavelength [nm]
2021-08-14T13:00
Radiance [W/m2/nm/sr]
Measurement
Approach 1
Approach 2
Approach 3
Wavelength [nm]
2021-09-02T13:00
Irradiance [W/m2/nm/sr]
Wavelength [nm]
2021-09-02T13:00
Radiance [W/m2/nm/sr]
Measurement
Approach 1
Approach 2
Approach 3
Wavelength [nm]

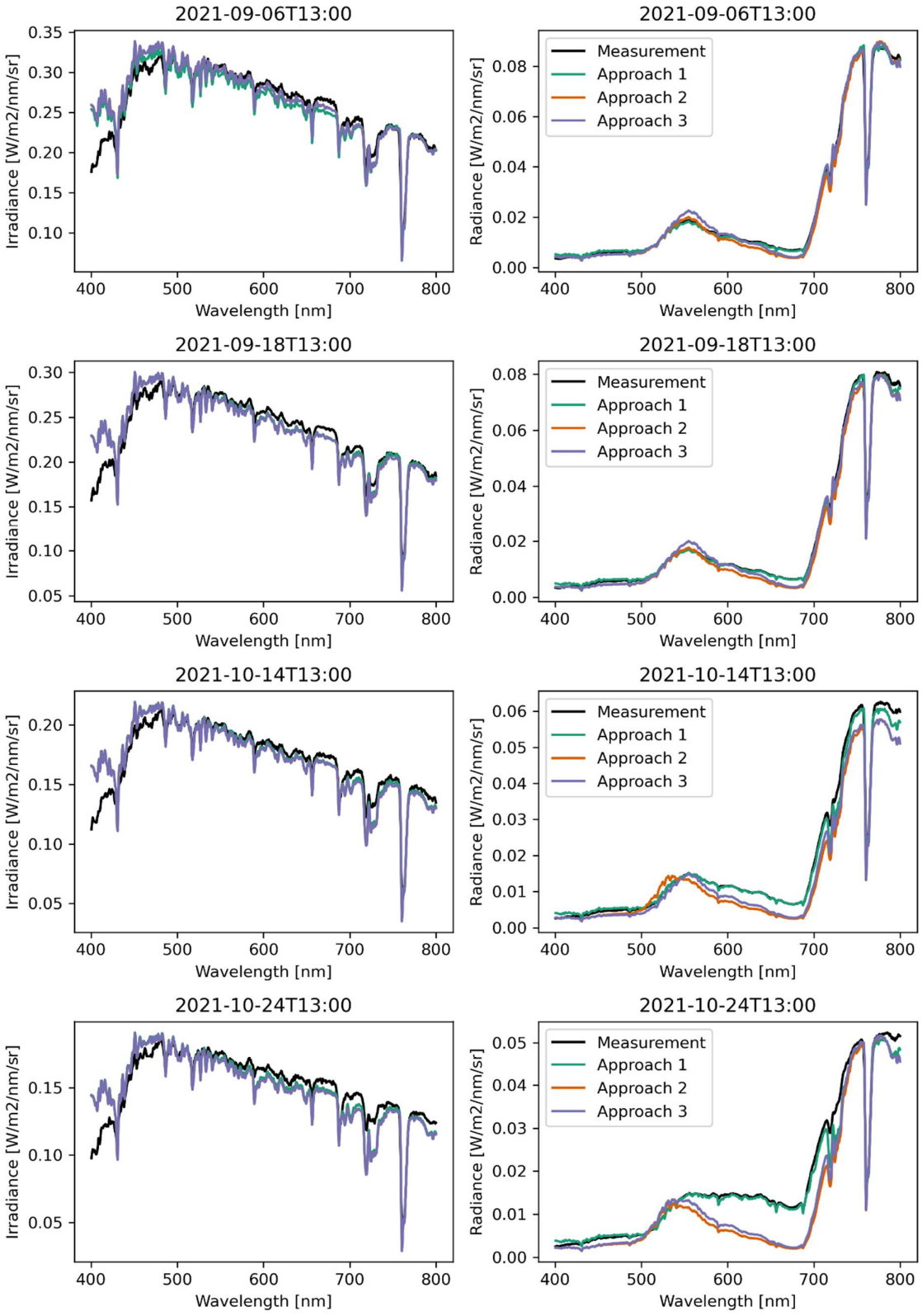

Figure 12: Irradiance (left) and radiance (right) simulations on sunny days over the period investigated by all approaches together with the measurement between 400 nm and 800 nm.

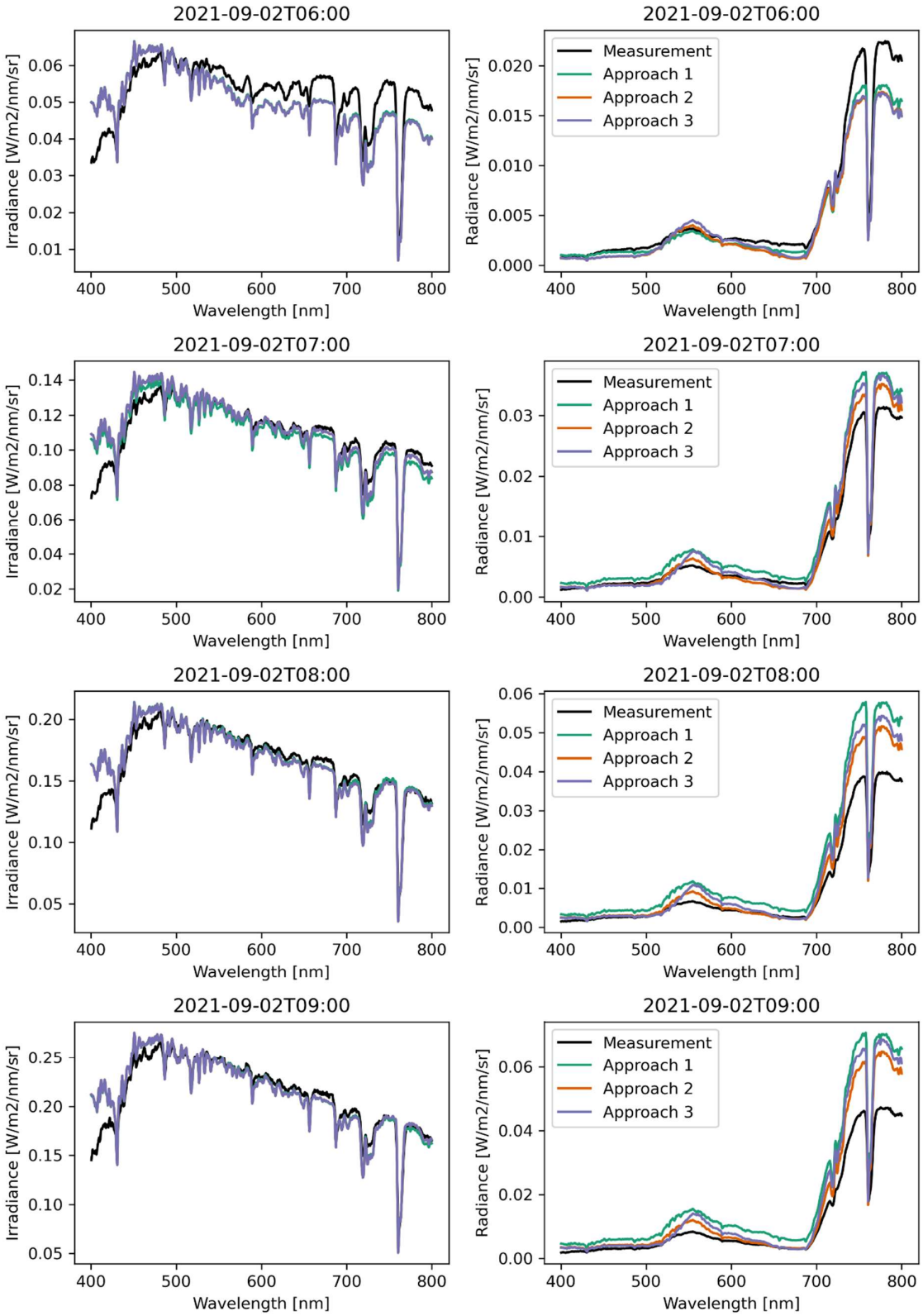
2021-09-02T06:00
Irradiance [W/m2/nm/sr]
Wavelength [nm]
2021-09-02T06:00
Radiance [W/m2/nm/sr]
Measurement
Approach 1
Approach 2
Approach 3
Wavelength [nm]
2021-09-02T07:00
Irradiance [W/m2/nm/sr]
Wavelength [nm]
2021-09-02T07:00
Radiance [W/m2/nm/sr]
Measurement
Approach 1
Approach 2
Approach 3
Wavelength [nm]
2021-09-02T08:00
Irradiance [W/m2/nm/sr]
Wavelength [nm]
2021-09-02T08:00
Radiance [W/m2/nm/sr]
Measurement
Approach 1
Approach 2
Approach 3
Wavelength [nm]
2021-09-02T09:00
Irradiance [W/m2/nm/sr]
Wavelength [nm]
2021-09-02T09:00
Radiance [W/m2/nm/sr]
Measurement
Approach 1
Approach 2
Approach 3
Wavelength [nm]

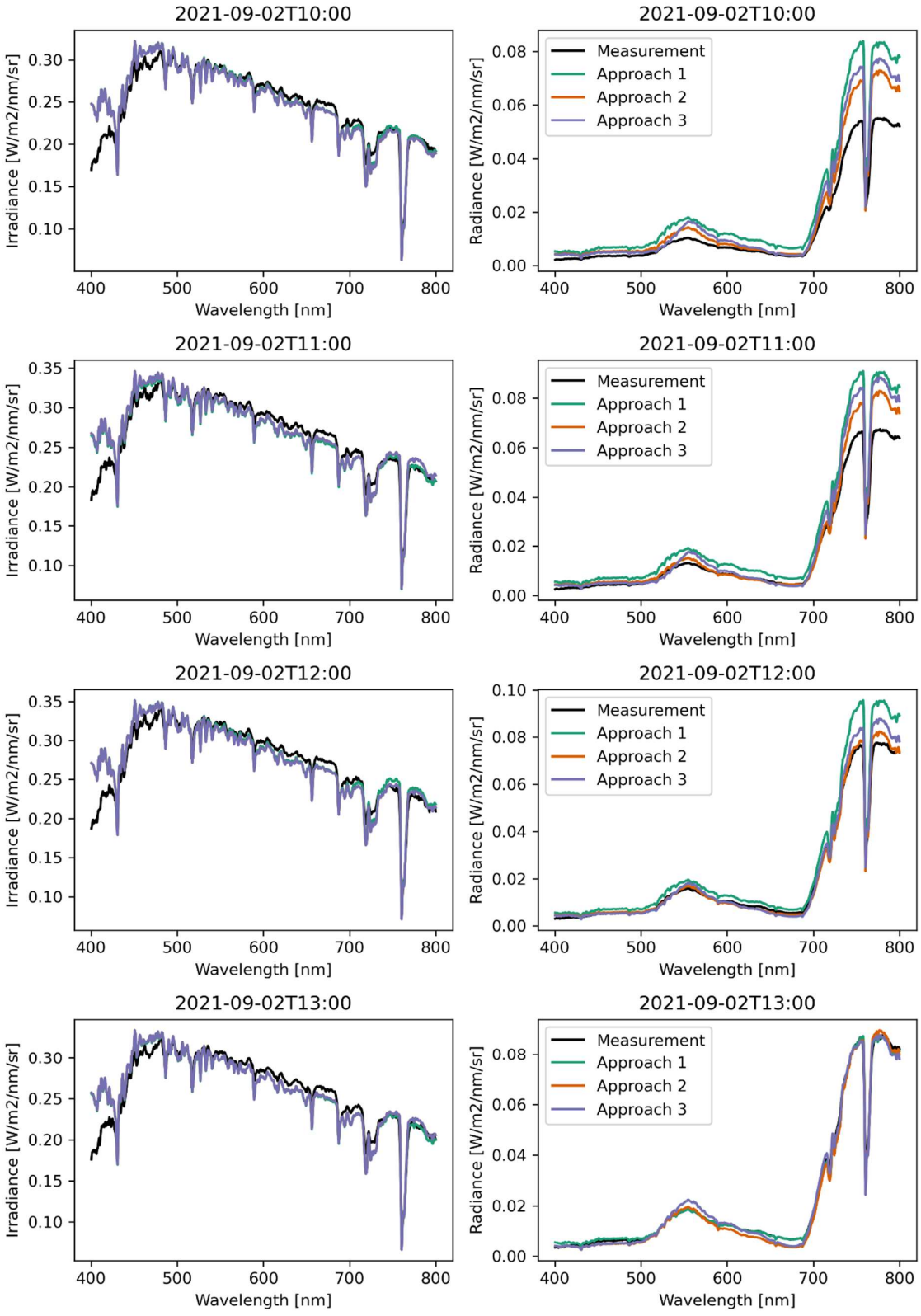
2021-09-02T10:00
Irradiance [W/m2/nm/sr]
Wavelength [nm]
2021-09-02T10:00
Radiance [W/m2/nm/sr]
Measurement
Approach 1
Approach 2
Approach 3
Wavelength [nm]
2021-09-02T11:00
Irradiance [W/m2/nm/sr]
Wavelength [nm]
2021-09-02T11:00
Radiance [W/m2/nm/sr]
Measurement
Approach 1
Approach 2
Approach 3
Wavelength [nm]
2021-09-02T12:00
Irradiance [W/m2/nm/sr]
Wavelength [nm]
2021-09-02T12:00
Radiance [W/m2/nm/sr]
Measurement
Approach 1
Approach 2
Approach 3
Wavelength [nm]
2021-09-02T13:00
Irradiance [W/m2/nm/sr]
Wavelength [nm]
2021-09-02T13:00
Radiance [W/m2/nm/sr]
Measurement
Approach 1
Approach 2
Approach 3
Wavelength [nm]

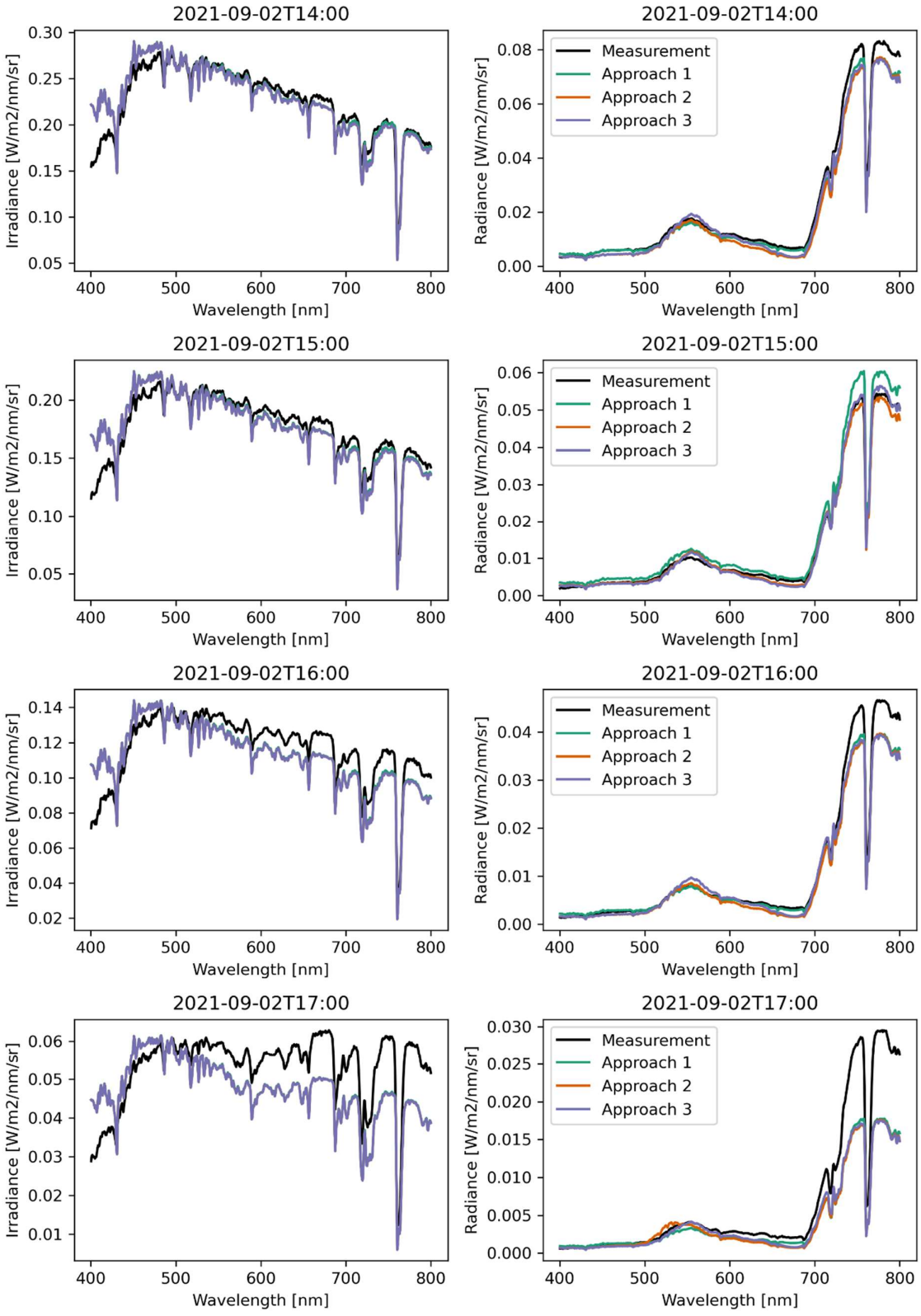

Figure 13: Results of irradiance (left) and radiance (right) simulations on the 2nd of September from 06:00 to 17:00 by all approaches together with the measurements from 400 nm to 800 nm.

References

Afuye, G.A., Kalumba, A.M., Busayo, E.T., Orimoloye, I.R., 2022. A bibliometric review of vegetation response to climate change. Environ. Sci. Pollut. Res. 29, 18578–18590.

Al Asmar, L., Musson-Genon, L., Dupont, E., Dupont, J.C., Sartelet, K., 2021. Improvement of solar irradiance modelling during cloudy-sky days using measurements. Sol. Energy 230, 1175–1188. https://doi.org/10.1016/J.SOLENER.2021.10.084

Alonso, K., Bachmann, M., Burch, K., Carmona, E., Cerra, D., de los Reyes, R., Dietrich, D., Heiden, U., Hölderlin, A., Ickes, J., Knodt, U., Krutz, D., Lester, H., Müller, R., Pagnutti, M., Reinartz, P., Richter, R., Ryan, R., Sebastian, I., Tegler, M., 2019. Data Products, Quality and Validation of the DLR Earth Sensing Imaging Spectrometer (DESIS). Sensors 2019, Vol. 19, Page 4471 19, 4471. https://doi.org/10.3390/S19204471

Atzberger, C., 2004. Object-based retrieval of biophysical canopy variables using artificial neural nets and radiative transfer models. Remote Sens. Environ. 93, 53–67. https://doi.org/10.1016/J.RSE.2004.06.016

Boccia, V., Adams, J., 2021. NASA-ESA Cooperation on the SBG and CHIME Hyperspectral Satellite Missions: a roadmap for the joint Working Group on Cal/Val activities.

Bouvet, M., Thome, K., Berthelot, B., Bialek, A., Czapla-Myers, J., Fox, N., Goryl, P., Henry, P., Ma, L., Marcq, S., Meygret, A., Wenny, B., Woolliams, E., 2019. RadCalNet: A Radiometric Calibration Network for Earth Observing Imagers Operating in the Visible to Shortwave Infrared Spectral Range. Remote Sens. 11, 2401. https://doi.org/10.3390/rs11202401

Brell, M., Guanter, L., Segl, K., Scheffler, D., Bohn, N., Bracher, A., Soppa, M.A., Foerster, S., Storch, T., Bachmann, M., Chabrillat, S., 2021. The EnMAP Satellite-Data Product Validation Activities. Work. Hyperspectral Image Signal Process. Evol. Remote Sens. 2021-March. https://doi.org/10.1109/WHISPERS52202.2021.9484000

Candela, L., Formaro, R., Guarini, R., Loizzo, R., Longo, F., Varacalli, G., 2016. The PRISMA mission, in: International Geoscience and Remote Sensing Symposium (IGARSS). https://doi.org/10.1109/IGARSS.2016.7729057

Cipar, J., Cooley, T., Lockwood, R., 2008. Measurements of seasonal changes in vegetation reflectance spectra. Int. Geosci. Remote Sens. Symp. 3, 812–815. https://doi.org/10.1109/IGARSS.2008.4779473

Cogliati, S., Sarti, F., Chiarantini, L., Cosi, M., Lorusso, R., Lopinto, E., Miglietta, F., Genesio, L., Guanter, L., Damm, A., Pérez-López, S., Scheffler, D., Tagliabue, G., Panigada, C., Rascher, U.,

Dowling, T.P.F., Giardino, C., Colombo, R., 2021. The PRISMA imaging spectroscopy mission: overview and first performance analysis. Remote Sens. Environ. 262. https://doi.org/10.1016/J.RSE.2021.112499

Craggs, G., 2016. Photosynthesis and its Role in Climate Change and Soil Regeneration. Futur. Dir. Int.

Cui, T., Sun, R., Xiao, Z., Liang, Z., Wang, J., 2020. Simulating spatially distributed solar-induced chlorophyll fluorescence using a BEPS-SCOPE coupling framework. Agric. For. Meteorol. 295, 108169. https://doi.org/10.1016/j.agrformet.2020.108169

Curran, P.J., Hay, A.M., 1986. The importance of measurement error for certain procedures in remote sensing at optical wavelengths. Photogrammetric Engineering & Remote Sensing

Damm, A., Erler, A., Hillen, W., Meroni, M., Schaepman, M.E., Verhoef, W., Rascher, U., 2011. Modeling the impact of spectral sensor configurations on the FLD retrieval accuracy of sun-induced chlorophyll fluorescence. Remote Sens. Environ. 115, 1882–1892. https://doi.org/10.1016/j.rse.2011.03.011

Despotovic, M., Nedic, V., Despotovic, D., Cvetanovic, S., 2016. Evaluation of empirical models for predicting monthly mean horizontal diffuse solar radiation. Renew. Sustain. Energy Rev. 56, 246–260. https://doi.org/10.1016/J.RSER.2015.11.058

Drusch, M., Moreno, J., Del Bello, U., Franco, R., Goulas, Y., Huth, A., Kraft, S., Middleton, E.M., Miglietta, F., Mohammed, G., Nedbal, L., Rascher, U., Schuttemeyer, D., Verhoef, W., 2017. The FLuorescence EXplorer Mission Concept-ESA's Earth Explorer 8. IEEE Trans. Geosci. Remote Sens. 55, 1273–1284. https://doi.org/10.1109/TGRS.2016.2621820

Eckardt, A., Horack, J., Lehmann, F., Krutz, D., Drescher, J., Whorton, M., Soutullo, M., 2015. DESIS (DLR Earth Sensing Imaging Spectrometer for the ISS-MUSES platform), in: International Geoscience and Remote Sensing Symposium (IGARSS). https://doi.org/10.1109/IGARSS.2015.7326053

Eugster, W., Zeyer, K., Zeeman, M.J., Michna, P., Zingg, A., Buchmann, N., Emmenegger, L., 2007. Methodical study of nitrous oxide eddy covariance measurements using quantum cascade laser spectrometry over a Swiss forest. Biogeosciences 4.

Feingersh, T., Dor, E. Ben, 2015. SHALOM - A Commercial Hyperspectral Space Mission, in: Optical Payloads for Space Missions. John Wiley & Sons, Ltd, Chichester, UK, pp. 247–263. https://doi.org/10.1002/9781118945179.ch11

Frappart, F., Wigneron, J.P., Li, X., Liu, X., Al-Yaari, A., Fan, L., Wang, M., Moisy, C., Le Masson, E., Lafkih, Z.A., Vallé, C., Ygorra, B., Baghdadi, N., 2020. Global Monitoring of the Vegetation

Dynamics from the Vegetation Optical Depth (VOD): A Review. Remote Sens. 2020, Vol. 12, Page 2915 12, 2915. https://doi.org/10.3390/RS12182915

Giardino, C., Bresciani, M., Braga, F., Fabbretto, A., Ghirardi, N., Pepe, M., Gianinetto, M., Colombo, R., Cogliati, S., Ghebrehiwot, S., Laanen, M., Peters, S., Schroeder, T., Concha, J.A., Brando, V.E., 2020. First Evaluation of PRISMA Level 1 Data for Water Applications. Sensors 2020, Vol. 20, Page 4553 20, 4553. https://doi.org/10.3390/S20164553

Gitelson, A.A., Zur, Y., Chivkunova, O.B., Merzlyak, M.N., 2002. Assessing Carotenoid Content in Plant Leaves with Reflectance Spectroscopy¶. Photochem. Photobiol. 75, 272.

Gorelick, N., Hancher, M., Dixon, M., Ilyushchenko, S., Thau, D., Moore, R., 2017. Google Earth Engine: Planetary-scale geospatial analysis for everyone. Remote Sens. Environ. 202, 18–27. https://doi.org/10.1016/j.rse.2017.06.031

Guanter, L., Kaufmann, H., Segl, K., Foerster, S., Rogass, C., Chabrillat, S., Kuester, T., Hollstein, A., Rossner, G., Chlebek, C., Straif, C., Fischer, S., Schrader, S., Storch, T., Heiden, U., Mueller, A., Bachmann, M., Mühle, H., Müller, R., Habermeyer, M., Ohndorf, A., Hill, J., Buddenbaum, H., Hostert, P., Van Der Linden, S., Leitão, P.J., Rabe, A., Doerffer, R., Krasemann, H., Xi, H., Mauser, W., Hank, T., Locherer, M., Rast, M., Staenz, K., Sang, B., 2015. The EnMAP Spaceborne Imaging Spectroscopy Mission for Earth Observation. Remote Sens. 2015, Vol. 7, Pages 8830-8857 7, 8830–8857. https://doi.org/10.3390/RS70708830

Guanter, L., Richter, R., Kaufmann, H., 2009. On the application of the MODTRAN4 atmospheric radiative transfer code to optical remote sensing. Int. J. Remote Sens. 30, 1407–1424. https://doi.org/10.1080/01431160802438555

Guanter, L., Zhang, Y., Jung, M., Joiner, J., Voigt, M., Berry, J.A., Frankenberg, C., Huete, A.R., Zarco-Tejada, P., Lee, J.E., Moran, M.S., Ponce-Campos, G., Beer, C., Camps-Valls, G., Buchmann, N., Gianelle, D., Klumpp, K., Cescatti, A., Baker, J.M., Griffis, T.J., 2014. Global and time-resolved monitoring of crop photosynthesis with chlorophyll fluorescence. Proc. Natl. Acad. Sci. U. S. A. 111. https://doi.org/10.1073/PNAS.1320008111

Hank, T.B., Berger, K., Bach, H., Clevers, J.G.P.W., Gitelson, A., Zarco-Tejada, P., Mauser, W., 2019. Spaceborne Imaging Spectroscopy for Sustainable Agriculture: Contributions and Challenges. Surv. Geophys. 40, 515–551.

Hosgood, B., Jacquemoud, S., Andreoli, G., Verdebout, J., Pedrini, G., Schmuck, G., 1994. Leaf Optical Properties EXperiment 93 (LOPEX93). Jt. Res. Cent.

Hueni, A., Damm, A., Kneubuehler, M., Schlapfer, D., Schaepman, M.E., 2017. Field and Airborne Spectroscopy Cross Validation -Some Considerations. IEEE J. Sel. Top. Appl. Earth Obs. Remote

Sens. 10, 1117–1135. https://doi.org/10.1109/JSTARS.2016.2593984

Iwasaki, A., Ohgi, N., Tanii, J., Kawashima, T., Inada, H., 2011. Hyperspectral Imager Suite (HISUI)-Japanese hyper-multi spectral radiometer, in: International Geoscience and Remote Sensing Symposium (IGARSS). https://doi.org/10.1109/IGARSS.2011.6049308

JB-Hyperspectral Devices UG, 2019. The Fluorescence Box , a hyperspectral instrument for unattended observation of chlorophyll fluorescence and reflectance . Manual for Installation and Operation.

Kattenborn, T., Erlangung, Z., Bau-, V.D.F., Umweltwissenschaften, G.-, Kit, T., 2018. Linking Canopy Reflectance and Plant Functioning through Radiative Transfer Models. Karlsruher Institut für Technologie (KIT).

Kattge, J., Bönisch, G., Díaz, S., 2020. TRY plant trait database – enhanced coverage and open access. Glob. Chang. Biol. 26, 119–188. https://doi.org/10.1111/gcb.14904

Kawabata, A., Ichii, K., Yamaguchi, Y., 2010. Global monitoring of interannual changes in vegetation activities using NDVI and its relationships to temperature and precipitation. 22, 1377–1382. https://doi.org/10.1080/01431160119381

Koetz, B., Member IEEE, Student, Sun, G., Member IEEE, Senior, Morsdorf, F., Ranson, K., Kneubühler, M., Itten, K., Allgöwer, B., 2006. Inversion of combined radiative transfer models for imaging spectrometer and LIDAR data. IEEE Xplore 395–398. https://doi.org/10.1109/IGARSS.2006.106

Kostkowski, H.J., 1997. Reliable Spectroradiometry, Spectroradiometry Consulting.

Laurent, V.C.E., Verhoef, W., Clevers, J.G.P.W., Schaepman, M.E., 2011. Estimating forest variables from top-of-atmosphere radiance satellite measurements using coupled radiative transfer models. Remote Sens. Environ. 115, 1043–1052. https://doi.org/10.1016/j.rse.2010.12.009

Laurent, V.C.E., Verhoef, W., Damm, A., Schaepman, M.E., Clevers, J.G.P.W., 2013. A Bayesian object-based approach for estimating vegetation biophysical and biochemical variables from APEX at-sensor radiance data. Remote Sens. Environ. 139, 6–17. https://doi.org/10.1016/j.rse.2013.07.032

Lauvernet, C., Baret, F., Hascoët, L., Buis, S., Le Dimet, F.X., 2008. Multitemporal-patch ensemble inversion of coupled surface-atmosphere radiative transfer models for land surface characterization. Remote Sens. Environ. 112, 851–861. https://doi.org/10.1016/J.RSE.2007.06.027

Li, S., Ganguly, S., Dungan, J.L., Wang, W., Nemani, R.R., 2017. Sentinel-2 MSI Radiometric Characterization and Cross-Calibration with Landsat-8 OLI. Adv. Remote Sens. 06, 147–159.

https://doi.org/10.4236/ARS.2017.62011

Lillesand, Kiefer, Chipman, 2015. Remote Sensing and Image Interpretation, Photogrammetric Engineering & Remote Sensing. https://doi.org/10.14358/pers.81.8.615

Liu, B., Do, P., Iung, B., Xie, M., 2020. Stochastic Filtering Approach for Condition-Based Maintenance Considering Sensor Degradation. IEEE Trans. Autom. Sci. Eng. 17, 177–190. https://doi.org/10.1109/TASE.2019.2918734

Malenovský, Z., Homolová, L., Lukeš, P., Buddenbaum, H., Verrelst, J., Alonso, L., Schaepman, M.E., Lauret, N., Gastellu-Etchegorry, J.P., 2019. Variability and Uncertainty Challenges in Scaling Imaging Spectroscopy Retrievals and Validations from Leaves Up to Vegetation Canopies. Surv. Geophys. 40, 631–656. https://doi.org/10.1007/S10712-019-09534-Y/FIGURES/5

Markham, B., Barsi, J., Kvaran, G., Ong, L., Kaita, E., Biggar, S., Czapla-Myers, J., Mishra, N., Helder, D., 2014. Landsat-8 Operational Land Imager Radiometric Calibration and Stability. Remote Sens. 2014, Vol. 6, Pages 12275-12308 6, 12275–12308. https://doi.org/10.3390/RS61212275

Mathworks, 2021. MATLAB Engine API [WWW Document]. URL https://ch.mathworks.com/help/matlab/matlab-engine-for-python.html (accessed 5.2.21).

Mayer, B., Kylling, A., 2005. Technical note: The libRadtran software package for radiative transfer calculations-description and examples of use. Atmos. Chem. Phys 5, 1855–1877.

Mayer, B., Kylling, A., Emde, C., Buras, R., Hamann, U., Gasteiger, J., Richter, B., 2017. libRadtran User ' s Guide. Ed. Libr. version 2.0.2.

Mohammed, G.H., Colombo, R., Middleton, E.M., Rascher, U., van der Tol, C., Nedbal, L., Goulas, Y., Pérez-Priego, O., Damm, A., Meroni, M., Joiner, J., Cogliati, S., Verhoef, W., Malenovský, Z., Gastellu-Etchegorry, J.P., Miller, J.R., Guanter, L., Moreno, J., Moya, I., Berry, J.A., Frankenberg, C., Zarco-Tejada, P.J., 2019. Remote sensing of solar-induced chlorophyll fluorescence (SIF) in vegetation: 50 years of progress. Remote Sens. Environ. 231, 111177. https://doi.org/10.1016/j.rse.2019.04.030

Mohammed, G.H., Noland, T.L., Irving, D., Sampson, P.H., Zarco-Tejada, P.J., Miller, J.R., 2000. Natural and stress-induced effects on leaf spectral reflectance in Ontario species Science Development and Transfer Ontario Ministry of Natural Resources.

Morley, P.J., Jump, A.S., West, M.D., Donoghue, D.N.M., 2020. Spectral response of chlorophyll content during leaf senescence in european beech trees. Environ. Res. Commun. 2. https://doi.org/10.1088/2515-7620/aba7a0

Morsdorf, F., Schneider, F., Gullien, C., Kükenbrink, D., Leiterer, R., Schaepman, M.E., 2020. The

Laegeren Site: An Augmented Forest Laboratory, in: Remote Sensing of Plant Biodiversity. pp. 1–581. https://doi.org/10.1007/978-3-030-33157-3

Nassar, A., Aboutalebi, M., McKee, M., Torres-Rua, A.F., Kustas, W., 2018. Implications of sensor inconsistencies and remote sensing error in the use of small unmanned aerial systems for generation of information products for agricultural management. Proc. SPIE--the Int. Soc. Opt. Eng. 10664, 1. https://doi.org/10.1117/12.2305826

Odorico, P.D.', Gonsamo, A., Damm, A., Schaepman, M.E., 2013. Experimental Evaluation of Sentinel-2 Spectral Response Functions for NDVI Time-Series Continuity. IEEE Trans. Geosci. Remote Sens. 51. https://doi.org/10.1109/TGRS.2012.2235447

Paul-Limoges, E., 2017. Biosphere-Atmosphere CO2 Exchange and its Link to Sun-Induced Fluorescence in a Mixed Forest and a Cropland. ETH. https://doi.org/10.3929/ethz-b-000250830

Petibon, F., Czyż, E.A., Ghielmetti, G., Hueni, A., Kneubühler, M., Schaepman, M.E., Schuman, M.C., 2021. Variation in reflectance spectroscopy of European beech leaves captures phenology and biological hierarchies despite measurement uncertainties. bioRxiv 2021.03.09.434578. https://doi.org/10.1101/2021.03.09.434578

Pricope, N.G., Husak, G., Lopez-Carr, D., Funk, C., Michaelsen, J., 2013. The climate-population nexus in the East African Horn: Emerging degradation trends in rangeland and pastoral livelihood zones. Glob. Environ. Chang. 23, 1525–1541. https://doi.org/10.1016/J.GLOENVCHA.2013.10.002

Process-based parallelism [WWW Document], 2022. URL https://billiard.readthedocs.io/en/latest/library/multiprocessing.html (accessed 5.24.22).

Quan, X., He, B., Li, X., 2015. A Bayesian Network-Based Method to Alleviate the Ill-Posed Inverse Problem: A Case Study on Leaf Area Index and Canopy Water Content Retrieval. IEEE Trans. Geosci. Remote Sens. 53, 6507–6517. https://doi.org/10.1109/TGRS.2015.2442999

Rivera, J.P., Verrelst, J., Gómez-Dans, J., Muñoz-Marí, J., Moreno, J., Camps-Valls, G., 2015. An Emulator Toolbox to Approximate Radiative Transfer Models with Statistical Learning. Remote Sens. 2015, Vol. 7, Pages 9347-9370 7, 9347–9370. https://doi.org/10.3390/RS70709347

Scartazza, A., Di Baccio, D., Bertolotto, P., Gavrichkova, O., Matteucci, G., 2016. Investigating the European beech (Fagus sylvatica L.) leaf characteristics along the vertical canopy profile: Leaf structure, photosynthetic capacity, light energy dissipation and photoprotection mechanisms. Tree Physiol. 36, 1060–1076. https://doi.org/10.1093/treephys/tpw038

Schaepman, M.E., Dangel, S., Kneubühler, M., Schläpfer, D., 2002. Quantitative Field Spectroscopic Measurement Instrumentation and Techniques, in: EPFS Workshop on Field Spectrometry. pp. 1–

12.

Shrestha, M., Helder, D., Christopherson, J., 2021. DLR earth sensing imaging spectrometer (Desis) level 1 product evaluation using radcalnet measurements. Remote Sens. 13. https://doi.org/10.3390/rs13122420

Stamnes, K., Tsay, S.-C., Wiscombe, W., Jayaweera, K., 1988. Numerically stable algorithm for discrete-ordinate-method radiative transfer in multiple scattering and emitting layered media. Appl. Opt. 27, 2502. https://doi.org/10.1364/ao.27.002502

Sterckx, S., Brown, I., Kääb, A., Krol, M., Morrow, R., Veefkind, P., Boersma, K.F., De Mazière, M., Fox, N., Thorne, P., 2020. Towards a European Cal/Val service for earth observation. Int. J. Remote Sens. 41, 4496–4511. https://doi.org/10.1080/01431161.2020.1718240

Sutter, F., Waldner, P., 2019. Laegeren research site [WWW Document]. URL https://www.envidat.ch/dataset/laegeren-research-site (accessed 6.22.21).

Thimonier Rickenmann, A., Schleppi, P., 2011. Blattflächenindex - WSL [WWW Document]. URL https://www.wsl.ch/de/ueber-die-wsl/versuchsanlagen-und-labors/lwf-demoflaeche/20-vegetation-und-biodiversitaet/24-lai.html (accessed 4.5.22).

Thompson, D.R., Guanter, L., Berk, A., Gao, B.C., Richter, R., Schläpfer, D., Thome, K.J., 2019. Retrieval of Atmospheric Parameters and Surface Reflectance from Visible and Shortwave Infrared Imaging Spectroscopy Data. Surv. Geophys. 40, 333–360.

Van Der Tol, C., Verhoef, W., Timmermans, J., Verhoef, A., Su, Z., 2009. An integrated model of soil-canopy spectral radiances, photosynthesis, fluorescence, temperature and energy balance. Biogeosciences 6, 3109–3129. https://doi.org/10.5194/BG-6-3109-2009

Verhoef, W., Bach, H., 2003. Remote sensing data assimilation using coupled radiative transfer models. Phys. Chem. Earth, Parts A/B/C 28, 3–13. https://doi.org/10.1016/S1474-7065(03)00003-2

Verrelst, J., Caicedo, J.P.R., Vicent, J., Pallarés, P.M., Moreno, J., 2019. Approximating Empirical Surface Reflectance Data through Emulation: Opportunities for Synthetic Scene Generation. Remote Sens. 2019, Vol. 11, Page 157 11, 157. https://doi.org/10.3390/RS11020157

Verrelst, J., Rivera Caicedo, J.P., Muñoz-Marí, J., Camps-Valls, G., Moreno, J., 2017. SCOPE-Based Emulators for Fast Generation of Synthetic Canopy Reflectance and Sun-Induced Fluorescence Spectra. Remote Sens. 2017, Vol. 9, Page 927 9, 927. https://doi.org/10.3390/RS9090927

Verrelst, J., Rivera, J.P., 2021. ARTMO v.3.29.

Walther, G.R., 2010. Community and ecosystem responses to recent climate change. Philos. Trans. R. Soc. B Biol. Sci. 365, 2019–2024. https://doi.org/10.1098/RSTB.2010.0021

Wang, D., Morton, D., Masek, J., Wu, A., Nagol, J., Xiong, X., Levy, R., Vermote, E., Wolfe, R., 2012. Impact of sensor degradation on the MODIS NDVI time series. Remote Sens. Environ. 119, 55–61. https://doi.org/10.1016/J.RSE.2011.12.001

Wang, J., Rich, P.M., Price, K.P., Kettle, W.D., 2010. Relations between NDVI and tree productivity in the central Great Plains. 25, 3127–3138. https://doi.org/10.1080/0143116032000160499

Wang, Z., Zhao, Y., Wang, B., 2018. A bibliometric analysis of climate change adaptation based on massive research literature data. J. Clean. Prod. 199, 1072–1082. https://doi.org/10.1016/J.JCLEPRO.2018.06.183

Yang, P., Prikaziuk, E., Verhoef, W., Van Der Tol, C., 2021. SCOPE 2.0: A model to simulate vegetated land surface fluxes and satellite signals. Geosci. Model Dev. 14, 4697–4712. https://doi.org/10.5194/gmd-14-4697-2021

Zebner, H., Zambelli, P., Taylor, S., Obinna Nwaogaidu, S., Michelson, T., Little, J., Lahmeyer, I., 2014. Pysolar [WWW Document]. URL https://pysolar.readthedocs.io/en/latest/ (accessed 5.24.22).

Zhou, L., Tucker, C.J., Kaufmann, R.K., Slayback, D., Shabanov, N. V., Myneni, R.B., 2001. Variations in northern vegetation activity inferred from satellite data of vegetation index during 1981 to 1999. J. Geophys. Res. Atmos. 106, 20069–20083. https://doi.org/10.1029/2000JD000115

Acknowledgements

I would like to thank Alex for consulting and supervising me during the thesis. The countless meetings helped to keep on the right track and were a great motivator as well as an excellent source of ideas and approaches to solving complicated problems. His comments on my drafts improved my writing style overall. I thank Veronika for her advice on radiative transfer. Her experience with libRadtran and SCOPE helped a lot. A big thank you goes to Bastian who mentored me during the thesis and was always willing to help whether it was conceptual coding or proofreading. Last but not least I would like to thank my family and friends for their advice and company throughout the creation of this work.

Personal Declaration

I hereby declare that the submitted thesis is the result of my own, independent work. All external sources are explicitly acknowledged in the thesis.

Place, Date

Zurich, 26.07.22

Signature